

Deep Foundation Capacity in Intermediate Geomaterials: A Database Study

Jean-Louis Briaud – Professor, Texas A&M University, College Station (TX, USA)
briaud@tamu.edu

Ali Doostvandi – PhD student, Texas A&M University, College Station (TX, USA)
alidoostvandi1@email.tamu.edu

ABSTRACT: Materials intermediate between soils and rocks are referred to as Intermediate Geo-Materials or IGM. They are earth materials that typically have SPT blow counts N between 50 and 200 bpf, unconfined compression strength σ_{CIR} between 0.5 and 5 MPa, and pressuremeter limit pressure p_L between 2.5 and 55 MPa. Deep foundations in IGM include bored piles (drilled shafts) and, less often, driven piles. The ultimate axial capacity of such deep foundations in IGM is studied in this article. A database of load tests on instrumented single piles with separate measurement of ultimate side shear stress f_u and ultimate point pressure p_u is assembled and analyzed. In tandem with the load test data, the IGM properties are collected including σ_{CIR} and N . Because the pressuremeter is thought to be the best tool for the characterization of IGM, values of p_L are obtained from correlation with σ_{CIR} . Correlation charts between f_u and p_u on one hand, and σ_{CIR} , N and p_L on the other, are generated to help the engineer select appropriate values of f_u and p_u for IGM. Furthermore, existing guidelines to estimate f_u and p_u in IGM are reviewed and evaluated against the database.

KEYWORDS: Intermediate Geo-Materials, weak rocks, stiff soils, strength, drilled shafts, ultimate friction, ultimate point pressure, load tests, database

Submitted: 10 November 2025; **Published:** 10 July 2026

Reference: Briaud, J.-L., & Doostvandi A. (2026). Deep Foundation Capacity in Intermediate Geomaterials: A Database Study. *ISSMGE International Journal of Geoengineering Case Histories*, 8(4), 31–53. <https://doi.org/10.4417/IJGCH-08-04-02>.

INTRODUCTION

Intermediate Geo-Materials, or IGM, are intermediate between soils and rocks. They straddle the fields of soil mechanics and rock mechanics. This creates a problem, as both fields do not use the same approaches to model the behavior of the material. For example, the consolidation theory exists in soil mechanics, but elasticity dominates in rock mechanics. Also soil strength is modeled differently in soils and in rocks. IGM varies widely, including highly compacted sand and gravel, tills, sandstones, weathered limestone, and weathered granite. Typically, these IGM exhibit Standard Penetration Test (SPT) N values between 50 and 200 bpf, and uniaxial compressive strengths in the range of 500 to 5000 kPa.

Shallow foundations are an option in IGM, as the IGM are usually quite strong. However, issues such as swelling, frost heave, heavy concentrated loads, or horizontal loads may require a deep foundation. The deep foundation of choice in IGM is drilled shafts; however, driven piles are sometime used. Their ultimate capacity requires estimating the ultimate side shear stress f_u and the ultimate point pressure p_u . Both f_u and p_u are typically obtained from correlations with IGM strength values such as the unconfined compression strength of IGM samples, which gives the unconfined compression strength of intact pieces of IGM, σ_{CIR} , or the Standard Penetration Test (SPT) blow count N , or the pressuremeter test (PMT) limit pressure p_L .

The work focused on a search for instrumented drilled shafts and driven piles load tests in weak rocks and stiff soils where the side friction and the point pressure were measured separately. The results obtained on those two topics are presented after some definitions and a review of existing knowledge.

DEFINITIONS AND CLASSIFICATIONS OF IGM

Definitions and classifications. According to O'Neill and Reese (1999), IGM can be classified in three categories:

1. *IGM Category I* are argillaceous geomaterials, including heavily over-consolidated hard clays, clay shales, claystone, siltstone, saprolites, and mudstones. The unconfined compressive strength (σ_{CIR}) of these materials typically falls between 500 and 5000 kPa and demonstrates a tendency for significant strength reduction upon exposure to water and to smearing when drilled.
2. *IGM Category II* are calcareous geomaterials including limestone, limerock, and argillaceous geomaterials not prone to smearing when drilled. Category II IGM are distinguished from Category I IGM, as the latter experience a compression strength loss of less than 40% of the original σ_{CIR} after being exposed to water for three days at 350 kPa confining pressure.
3. *IGM Category III* are highly compact granular geomaterials, including residual rock fragments, fully decomposed rock, and glacial till. Standard Penetration Test (SPT) values typically range between 50 and 200 blows per 0.3 meters.

IGM mass indices. Some of the rock mass indices are useful in IGM. They are the Recovery Ratio (RR %), defined as the length of core recovered divided by the length cored expressed as a percentage, and the Rock Quality Designation (RQD %), defined as the cumulative length of core segments longer than 0.1 m divided by the length cored expressed as a percentage (Deere, 1964). The classification systems which help evaluate the relationship between the intact rock and the rock mass are the rock mass rating (RMR) (Bieniawski, 1989), the Geologic Strength Index (GSI) (Hoek, 1994) and the Q slope rating (Q) (Barton et al., 1974).

IGM tests. The tests involved in characterizing the properties of these IGMs are laboratory tests and in situ tests. The assumption is that the laboratory test defines the intact IGM parameters, while the in situ test defines the IGM mass parameters. This is based on the volume of material tested with the lab test being about 0.0007 m³ (e.g.: unconfined compression), and the in situ test about 1 m³ (e.g.: pressuremeter) or 1500 times more IGM mass volume. As such, the in situ test is likely to give the IGM mass modulus, E_{RM} , and the IGM mass unconfined compression strength, σ_{CRM} , while the lab test gives the intact IGM modulus, E_{IR} , and the intact IGM unconfined compression strength, σ_{CIR} . The laboratory tests include the Unconfined Compression Test (UCT) and the tension strength test (TST), also known as the Brazilian test. The in situ tests include the Flat Jack Test (PJT) (Deklotz and Boisen, 1970), the Plate Load Test (PLT) (Bieniawski, 1981), the Radial Jacking Test (RJT) also known as the Goodman Jack Test (Goodman et al., 1968), and the Pressuremeter Test (PMT) (Briaud, 1992). These in situ tests aim to measure the IGM modulus in situ but rarely give the IGM strength. The rock borehole shear test (RBST) (Yang et al., 2006) aims to measure the in-situ shear strength parameters. It is recognized that the distinction between intact and IGM mass properties is not governed solely by specimen volume but is also a function of scale effects and material structure, including bedding, fissuring, jointing, and degree of weathering. While laboratory specimens are commonly interpreted as representing intact IGM behavior, some specimens—particularly those obtained from highly fractured or laminated IGMs—may already reflect structural features and therefore behave closer to an IGM mass response. In this study, laboratory and in situ test results are interpreted as specimen-scale and mass-scale properties, respectively, following a practical engineering framework rather than a strict theoretical separation.

EXISTING KNOWLEDGE

Existing guidelines regarding drilled shafts capacity and IGM were reviewed. Brown et al. (2010) provides one of the major sets of recommendations. They propose the following equations for the ultimate side shear stress f_u and the ultimate point pressure p_u of IGM and rock. Different equations apply to different materials as follows:

$$f_u = \alpha_1 \varphi_1 \sigma_{CIR}; \text{ cohesive IGM such as argillaceous rock including shale, claystone, siltstone} \quad (1)$$

$$\frac{f_u}{p_a} = 0.65 \alpha_E \sqrt{\frac{\sigma_{CIR}}{p_a}}; \text{ rock} \quad (2)$$

$$f_u(ksf) = 0.075N; \text{ soil-like claystone} \quad (3)$$

$$f_u(ksf) = 2.05 \sigma_{CIR}(ksf)^{0.5}; \text{ very hard sandy claystone} \quad (4)$$

$$p_u(ksf) = 17 \sigma_{CIR}(ksf)^{0.51}; \text{ very hard sandy claystone} \quad (5)$$

$$p_u(ksf) = 0.92N; \text{ soil-like claystone} \quad (6)$$

Where α_1 is an empirical factor ranging from 0.07-0.5 depending on the unconfined compression strength of the IGM and the concrete fluid pressure at time of pouring, φ_1 is a correction factor for the degree of jointing ranging from 0.45 to 1.0 depending on the RQD (from 20-100%), σ_{CIR} is the unconfined compressive strength of the intact rock, α_E is a function of the ratio of the rock mass modulus over the intact rock modulus with a range of 0.45 to 1.0, and N is the SPT blow count. In the evaluation section of this article the following average factors were considered: $\alpha_1 = 0.25$ and $\varphi_1 = 0.55$ for $RQD = 50\%$, $\alpha_E = 0.45$ for $RQD = 20\%$, $\alpha_E = 0.55$ for $RQD = 70\%$. AASHTO (1998), as quoted by Abu-Hejleh (2003), mentions the following relationship (Equation 7) between f_u and N for cohesionless IGM (Category 3 of O'Neill et al. ,1996). Then, O'Neill and Reese (1999), as quoted by Abu-Hejleh (2003), updated this relationship by using the vertical effective stress parameter (Equation 8).

$$f_u(ksf) = 0.044(N - 53) + 3.1 \quad \text{for } N > 53 \quad (7)$$

$$f_u(ksf) = 1.07 \sigma'_v(ksf)^{0.2} N^{0.8} \quad \text{for } 53 < N < 100 \quad (8)$$

Where σ'_v is the vertical effective stress in the middle of the layer. After analyzing a database of drilled shaft load tests on soft and horizontally jointed rock with RQD values between 70 and 100, and with an unconfined compression strength $\sigma_{CIR} > 0.5$ MPa, Zhang and Einstein (1998) recommended the following formula for the ultimate point pressure:

$$p_u(ksf) = 21.4 \sigma_{CIR}(ksf)^{0.51} \quad (9)$$

O'Neil and Reese (1999) recommend the following equation to estimate the ultimate point pressure for cohesive IGM as well as massive rock with an RQD equal to 100% and a socket depth larger than 1.50 B where B is the socket width.

$$p_u(MPa) = 2.5 \sigma_{CIR}(MPa) \quad (10)$$

The SETRA French manual (2009) provides recommendations for drilled shafts in rock.

$$f_u(MPa) = \lambda \sqrt{\sigma_{CIR}(MPa)} \quad (11)$$

$$p_u(MPa) = 2 \alpha_2 \sqrt{\sigma_{CIR}(MPa)} \quad (12)$$

where λ depends on the roughness of the pile-IGM interface and varies from 0.15 to 0.25, and α_2 is a weathering factor depending on the RQD with values of 2.00 for RQD = 100% and 0.12 for RQD < 10%. In the evaluation section of this article, the following parameter values were chosen: $\lambda = 0.15$ and 0.25 , $\alpha_2 = 0.12, 1.00$, and 2.00 . Another French guidance document (Norme AFNOR, 2013) provides steps to estimate the ultimate side shear stress f_u . The steps include categorizing the soil and IGM material into five groups, then selecting the pile type, then choosing the appropriate design curve, then reading f_u corresponding to the PMT limit pressure p_L on that curve. The three curves are Q3 for chalk, Q4 for marl and marly limestone, and Q5 for weathered rock. This document also gives the ultimate point pressure p_u as:

$$p_u = k_p p_L + \gamma d \quad (13)$$

Where k_p is the PMT bearing capacity factor, γ is the soil total unit weight, and d is the depth of embedment of the pile. The value of k_p in Equation 13 for most IGM in the guidelines is 1.45. The Canadian Foundation Engineering Manual (CFEM, 2006) suggests the following relations between the ultimate side shear stress f_u , the point resistance p_u , and the unconfined compression strength σ_{CIR} of a soil, IGM, and rock.

$$\frac{f_u}{p_a} = b \left(\frac{\sigma_{CIR}}{p_a} \right)^{0.5}; \text{ IGM and Rock} \quad (14)$$

$$p_u = 3K_{sp} d \sigma_{CIR}; \text{ IGM and Rock} \quad (15)$$

Where p_a is the atmospheric pressure, b is an empirical factor with a lower bound of 0.63 and an average of 1.41, K_{sp} is an empirical factor ranging from 0.1 to 0.4, and d is depth factor equal to $1 + 0.4 L_s/B_s \leq 3$ in which L_s is the socket length and B_s is the socket diameter.

Existing guidelines regarding driven piles in IGM were reviewed. Adhikari et al. (2020) used a database of 17 steel-H piles driven into IGM called WyoPile. The purpose was to develop an extended α -method to estimate the ultimate side shear stress f_u . The following relation was proposed:

$$f_u(ksf) = \alpha' \sigma_{CIR}(ksf) \quad (16)$$

$$\text{Where } \alpha' = \frac{64.63 \sigma_{CIR}(ksf)^{-0.66}}{100}$$

Meyerhof (1976), as quoted by Long (2016), proposed the following formulas to predict the ultimate side shear stress f_u for low-displacement driven piles in cohesionless IGM (Equation 17). He also recommended a correlation (Equation 18) for the ultimate point pressure p_u of driven piles in sand using the SPT N values.

$$f_u(ksf) = N_{60}/50 \quad (17)$$

$$p_u(tsf) = 4N_{60} \quad (18)$$

Brown (2001), as quoted by FHWA-NHI (2016), came up with the following formula for the point resistance of driven piles using the SPT N_{60} values for materials ranging from soil to IGM ($SPT N_{60} < 100$):

$$p_u(ksf) = 3.55N_{60} \quad (19)$$

Rehman and Broms (1971), as quoted by Morton (2012), suggested that the point resistance of flat rock surfaces with a minimum pile embedment can be estimated by the following equation.

$$p_u = 4 \text{ to } 6 \sigma_{CIR} \quad (20)$$

The factor 5 was considered in the evaluation section of this paper.

Masud et al. (2024) employed CAPWAP to determine the ultimate side shear stress f_u and ultimate point pressure p_u of driven piles based on the SPT blow count and the unconfined compressive strength of IGMs. They used the results of 39 pile load tests from 28 bridge projects to gather a database. Since they encountered a variety of IGM materials, they came up with distinct relationships for each IGM type as expressed below:

$$f_u(MPa) = 7.5p_a e^{-4.51^{43}/N}; \text{ (Granite)} \quad (21)$$

$$f_u(MPa) = 0.42p_a \left(\frac{N_1}{16}\right)^{0.63}; \text{ (Siltstone)} \quad (22)$$

$$f_u(MPa) = 0.082 \sigma_{CIR}(MPa)^{0.44}; \text{ (Siltstone)} \quad (23)$$

$$f_u(MPa) = 0.09 \sigma_{CIR}(MPa)^{0.29}; \text{ (Claystone)} \quad (24)$$

$$f_u(MPa) = 0.08 \sigma_{CIR}(MPa)^{0.37}; \text{ (Sandstone)} \quad (25)$$

$$p_u(MPa) = 6.64 \sigma_{CIR}(MPa)^{0.42}; \text{ (Claystone)} \quad (26)$$

$$p_u(MPa) = 12.9P_a \left[2.43 \left(\frac{9.88N}{30D_B}\right)\right]; \text{ (Siltstone)} \quad (27)$$

Where D_B is the pile embedment depth with $2.13 < \frac{N}{D_B} < 11.13$. All the predictions made according to the equations mentioned in this section are later presented by comparing the predictions with the measurements for the assembled database of pile load tests. The assembled database for drilled shafts is described next.

CAPACITY OF DRILLED SHAFTS IN IGM

A database of drilled shaft load tests in IGM was assembled from several sources. They included the load tests described in the appendices of the FHWA drilled shaft manual (Brown et al., 2010), load tests from documents publicly available (Stark et al., 2017; Zhang, 2004; Williams and Pells, 1981), and load tests contributed by company members of the Consortium for Education and Research in Geo-Engineering Practice (CERGEP) at Texas A&M University. The requirements were that the load tests should be on instrumented piles where the side friction and the point resistance were measured separately, that the IGM would be described including strength measurements, and that the top movement of the pile would move downward approximately one tenth of the pile diameter. A total of 318 such load tests were collected and organized with 143 from Zhang (2004), 68 from William and Pells (1981), 65 from Stark et al. (2017), 20 from FHWA (2010), 16 from ECS, and 6 from CORSAIR. They lead to 483 values of the ultimate side shear stress f_u and 84 values of the ultimate point pressure p_u . The strength of the IGM was typically given by its SPT blow count N in blows per foot (bpf) or by the unconfined compression strength of the intact IGM, σ_{CIR} .

The ultimate side shear stress f_u was then plotted against the strength parameter of the IGM (N or σ_{CIR}). These plots are in Figures 1 and 2. The scatter is obvious but so is the trend. The mean regression line was identified and gave the following equations.

$$f_u(MPa) = 0.218(\sigma_{CIR}(MPa))^{0.719} \quad (28)$$

$$f_u(MPa) = 0.00209(N(bpf))^{1.02} \quad (29)$$

Upper and lower bounds with associated equations are shown on the plots corresponding to plus and minus one standard deviation of the data. The ± 1 standard deviation (S.D.) lines shown in the figures represent the variability of the measured data around the regression model. The S.D. was computed based on the residuals between measured and predicted (regression) values. In engineering terms, these bounds provide a practical representation of the uncertainty inherent in Intermediate GeoMaterials (IGMs), which exhibit natural heterogeneity and testing variability. These bounds allow engineers to account for uncertainty in design and to select conservative or representative values depending on the design philosophy adopted. Note that the data for soils and the data for rocks is included in the figures along with the IGM data to emphasize the continuity of the relationship between all three main categories of earth materials.

In Figure 1, the space bounded by the IGM limits and by the upper and lower standard deviation best fit lines was studied to try to detect any influence of the type of IGM on the value of f_u . The type of IGM was mentioned in the published documents used to collect the database. Unfortunately, a definite lack of consistency in the definition and description of these IGM types and the scatter in the data did not permit identifying specific zones where specific IGM types could be located. Furthermore, zoning that space in terms of RQD failed because not enough f_u and p_u data was associated with RQD values. However, the degree of weathering expressed in words in the published documents allowed some zoning. The terms slightly weathered, moderately weathered, and highly weathered were identified as IGM categories. Figure 3 shows a separation by colors of the three types of weathering for the IGM. It indicates that the highly weathered IGMs are mostly in the lower third of that space, the moderately weathered IGM in the middle third of that space, and the slightly weathered IGM in the top third of that space. An attempt at defining the degree of weathering is outlined below:

- *Slightly weathered*: discontinuities are well-defined, clean, and relatively widely spaced.
- *Moderately weathered*: discontinuities are more closely spaced, and weathering begins to reduce the strength of the material between discontinuities.
- *Highly weathered*: Discontinuities are close together and irregular; the pattern of fractures or joints forms a network, and merges into a highly fractured or disintegrated material.

The ultimate point pressure p_u was obtained from the load tests. However, it was not always clear if the drilled shaft point had plunged or not during such high-load load tests. If the publication used stated that the pressure reached was the ultimate point pressure the data was used as such. If the load transfer curve at the drilled shaft point was given and reached a minimum of 25 mm displacement, that p_u value was used. If not, that p_u value was not used. The collected p_u values were plotted against the strength parameter of the IGM (N or σ_{CIR}). These plots are in Figures 4 and 5 and the associated mean regression equations are below. The p_u and N_c points with an upward arrow in Figures 4, 5, 7, 10, 11, and 13 indicate that the measured values were not stated in the publications as ultimate values, but rather as the maximum measured values. These data are not incorporated in calculating the regression line since they had not plunged or reached the minimum of 25 mm displacement. The p_u and N_c points with open circles indicate the extrapolated ultimate pressure and are incorporated in finding the regression line.

$$p_u(\text{MPa}) = 4.48(\sigma_{CIR}(\text{MPa}))^{0.521} \quad (30)$$

$$p_u(\text{MPa}) = 1.13(N)^{0.247} \quad (31)$$

The authors are of the opinion that the pressuremeter (PMT) is one of the best tools to obtain useful parameters for the design of deep foundations in IGM. For that reason, an effort was made to generate plots of f_u vs p_L and p_u vs p_L where p_L is the PMT limit pressure. Because no PMT data was associated with any of the load tests collected, estimates of the limit pressure were obtained from the values of σ_{CIR} using the correlation developed by Briaud (1992). Note that these equations were developed for soils up to 500 kPa unconfined compression strength and 2000 kPa PMT limit pressure.

$$\sigma_{CIR}(\text{kPa}) = 1.34(p_L(\text{kPa}))^{0.75} \quad \text{or} \quad p_L(\text{kPa}) = 0.677(\sigma_{CIR}(\text{kPa}))^{1.33} \quad (32)$$

Then the plots of f_u vs p_L and p_u vs p_L could be generated as shown in Figures 6 and 7. The mean regression equations are:

$$f_u(\text{MPa}) = 0.0818(p_L(\text{MPa}))^{0.538} \quad (33)$$

$$p_u(\text{MPa}) = 2.14(p_L(\text{MPa}))^{0.399} \quad (34)$$

Note that Equation 34 indicates that the ultimate point pressure would be much smaller than the PMT limit pressure. This is surprising and doubt remains on whether the load test data gives the ultimate point pressure at failure. Indeed, it seems logical to use the PMT limit pressure as the ultimate point bearing pressure under a pile.

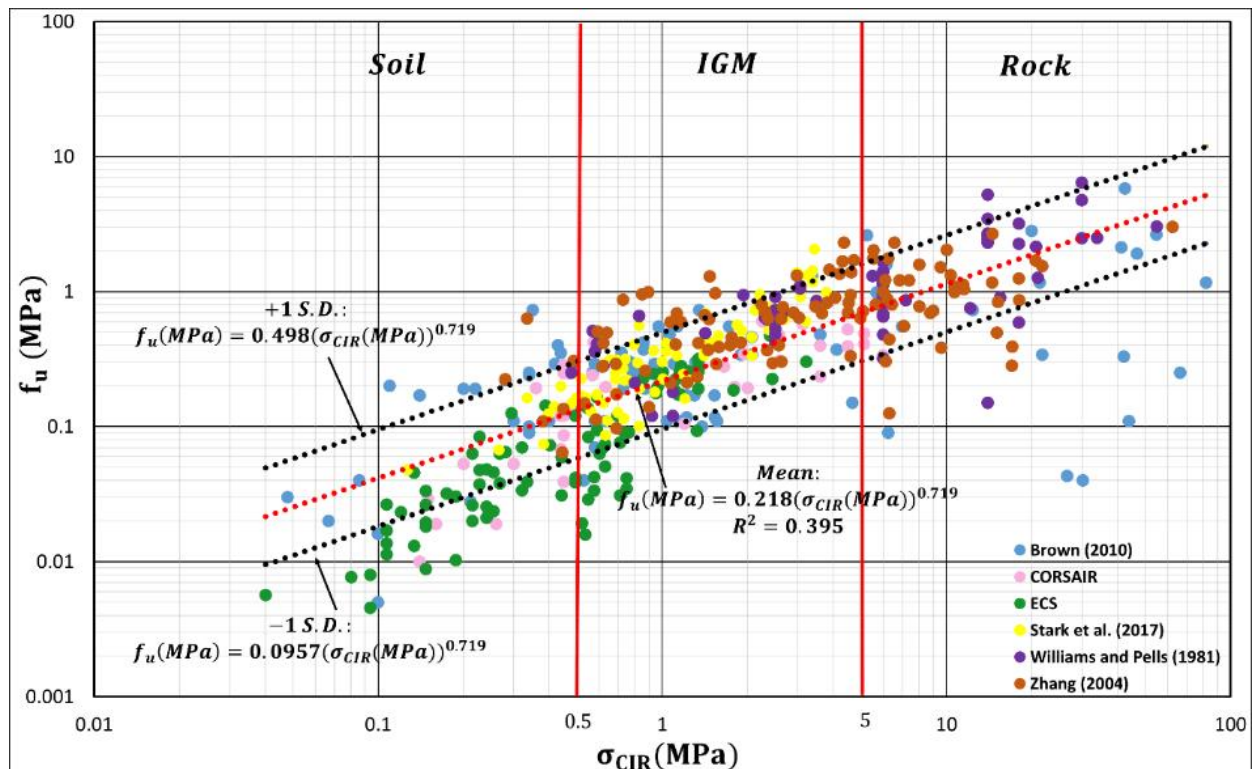


Figure 1. Ultimate side shear stress f_u versus unconfined compression strength σ_{CIR} for drilled shafts in IGM.

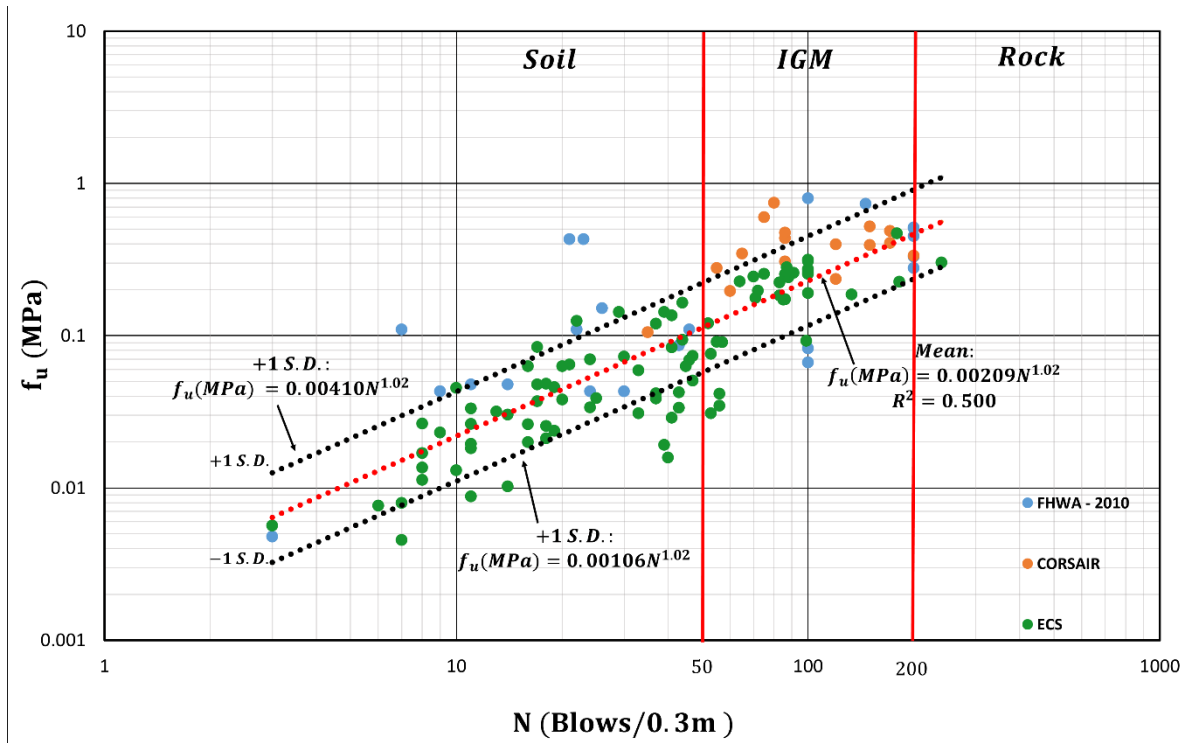


Figure 2. Ultimate side shear stress f_u versus SPT blow count N for drilled shafts in IGM.

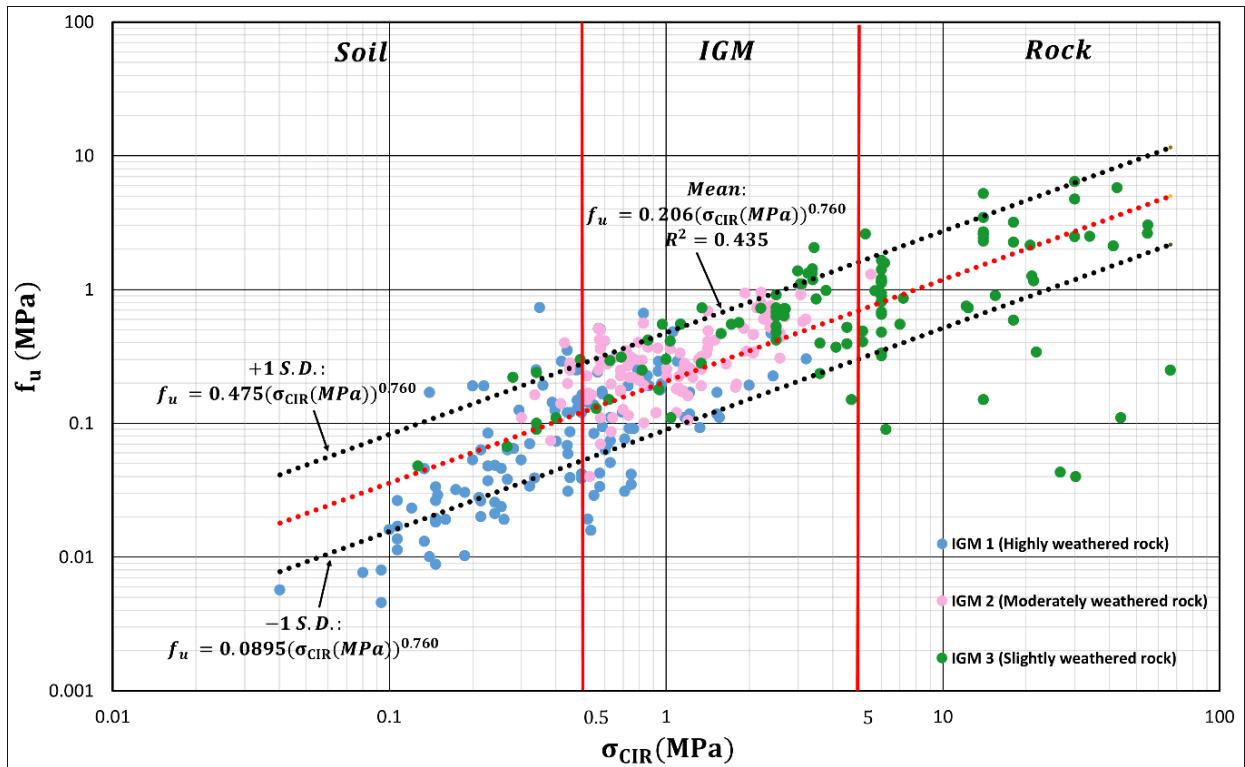


Figure 3. Influence of degree of weathering on the ultimate side shear stress f_u versus unconfined compression strength σ_{CIR} for drilled shafts in IGM.

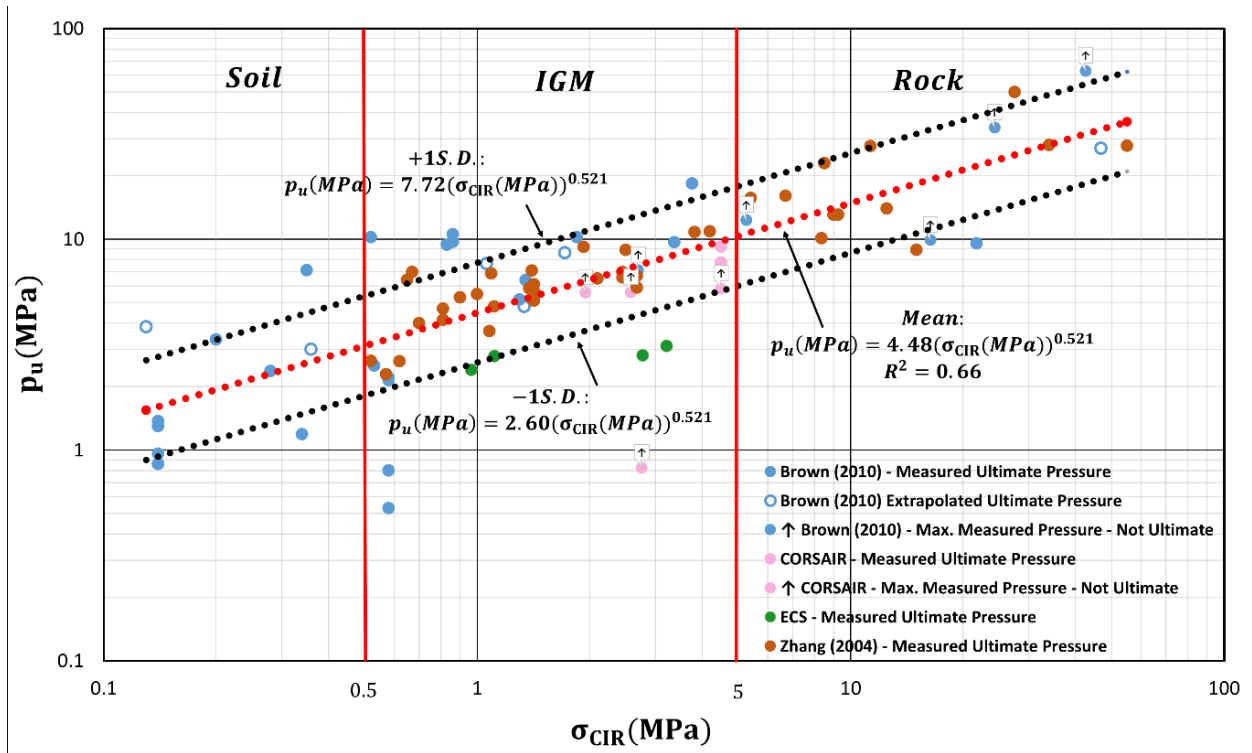


Figure 4. Ultimate point pressure p_u versus unconfined compression strength σ_{CIR} for drilled shafts in IGM.

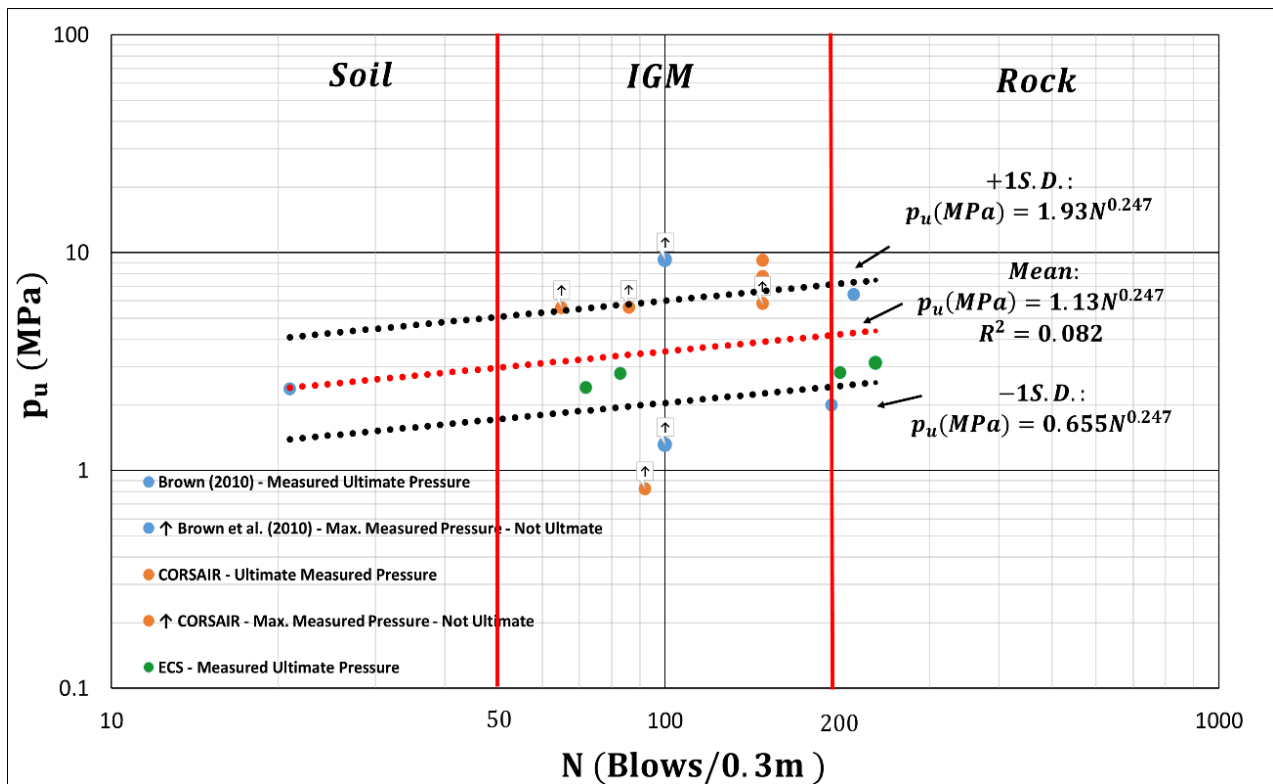


Figure 5. Ultimate point pressure p_u versus SPT blow count N for drilled shafts in IGM.

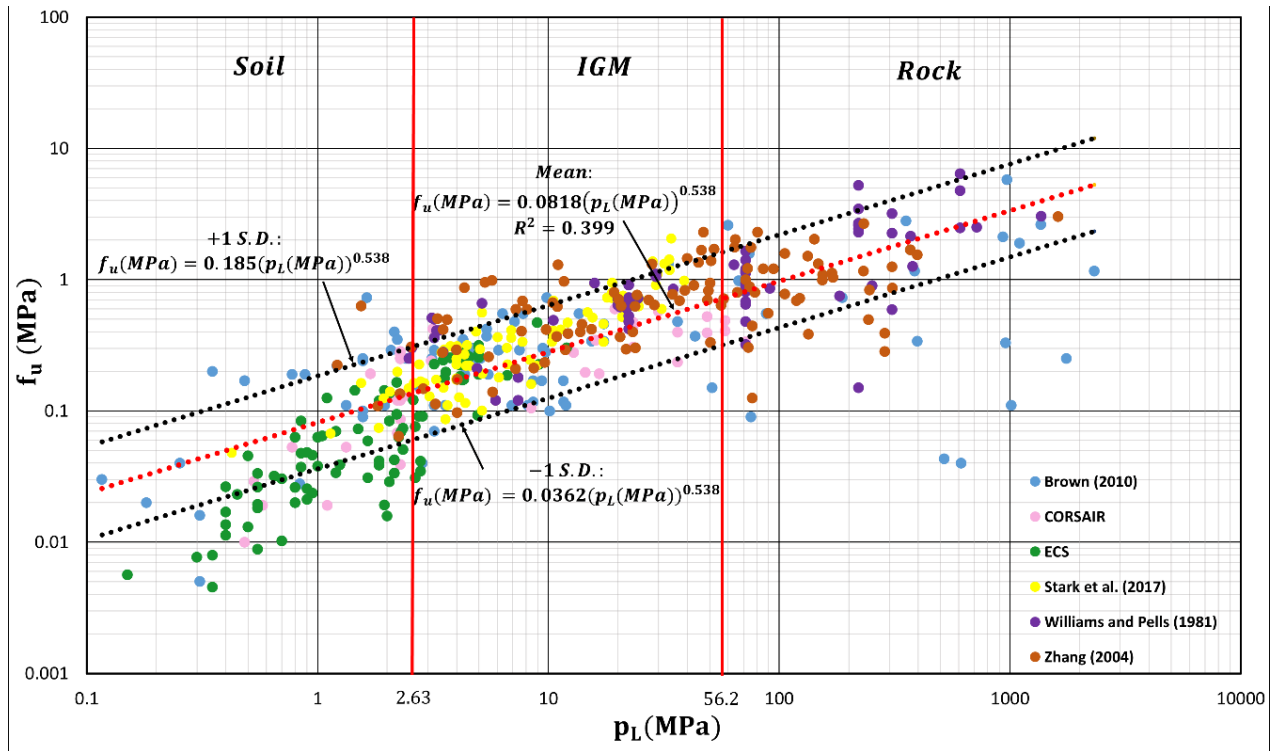


Figure 6. Ultimate side shear stress f_u versus pressuremeter limit pressure p_L for drilled shafts in IGM.

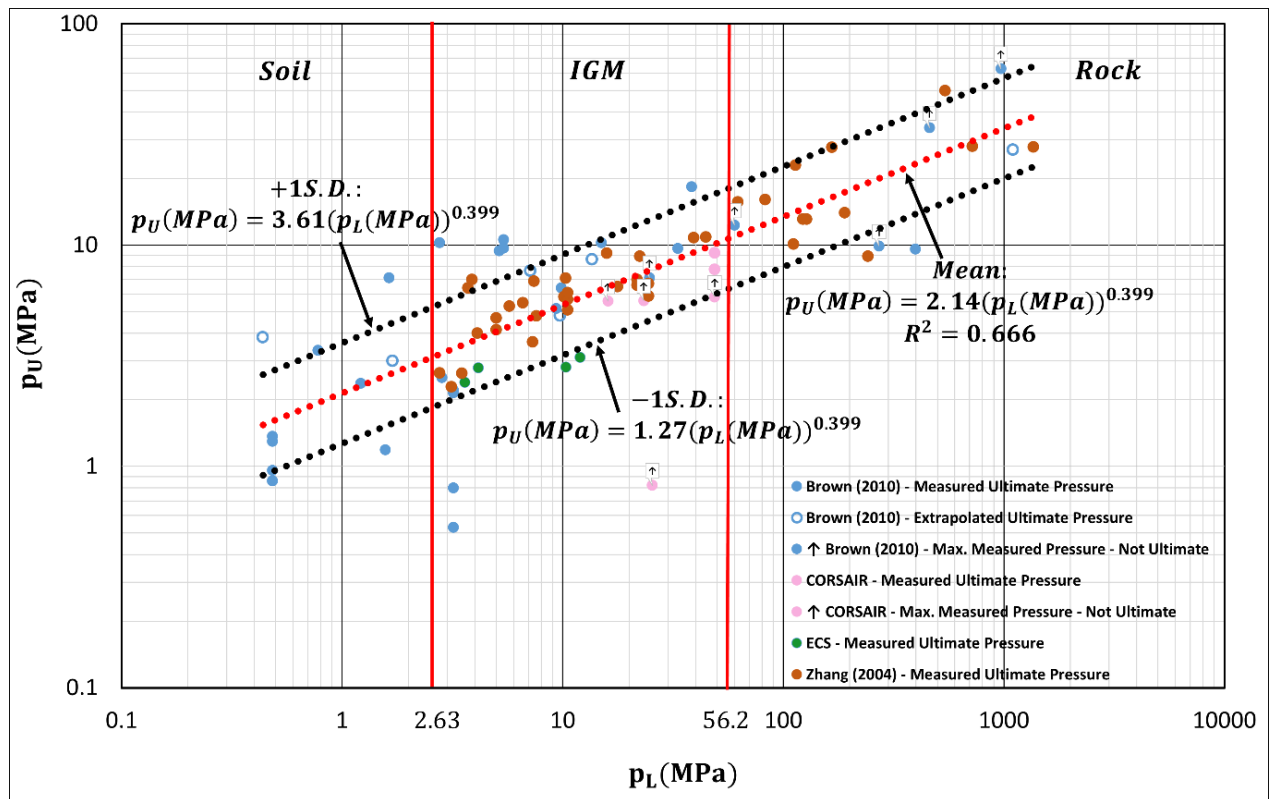


Figure 7. Ultimate point pressure p_u versus pressuremeter limit pressure p_L for drilled shafts in IGM.

EVALUATION OF EXISTING GUIDELINES FOR DRILLED SHAFTS IN IGM

Guidelines have been developed for drilled shafts in IGM, as described earlier. Some of these guidelines can now be evaluated against the database. For clay soils, f_u is usually correlated to the undrained shear strength, which is $\sigma_{CIR}/2$. In that practice, the factor α is defined as the ratio of $f_u/(\sigma_{CIR}/2)$. For soils, the parameter α is typically taken as 0.55 for drilled shafts until the undrained shear strength reaches 150 kPa and then decreases beyond that. The data in this database (Figure 8) indicates that the parameter α continues to decrease for IGM and for rocks. Other guidelines to obtain f_u from IGM parameters have been described in the existing knowledge section. The curves corresponding to the equations in those recommendations are presented in Figure 9 along with the data collected. As can be seen, some guidelines are conservative while others are optimistic. This figure helps the engineer to decide which prediction equations to use.

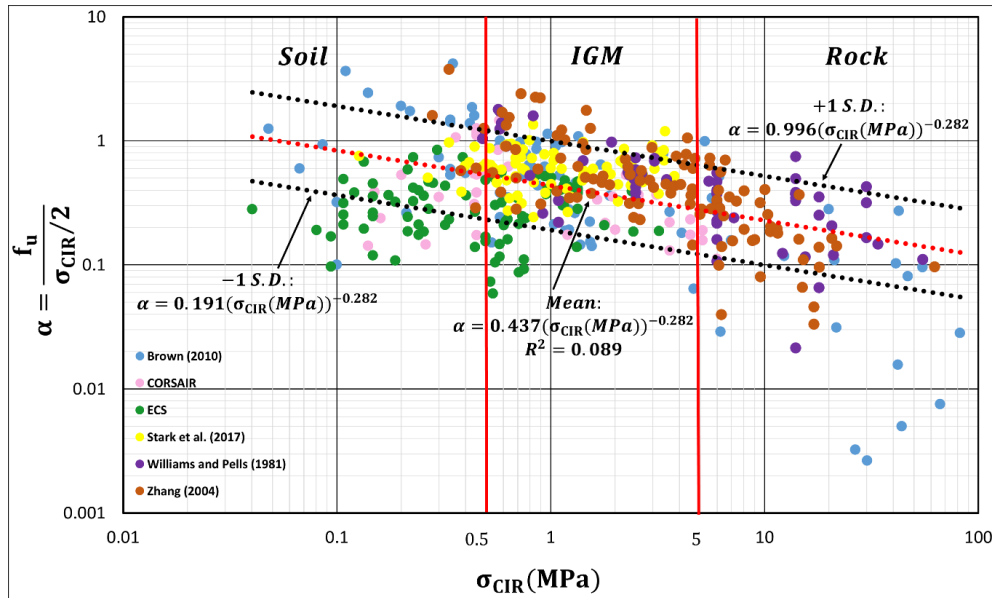


Figure 8. Parameter α vs the unconfined compression strength σ_{CIR} for drilled shafts in IGM.

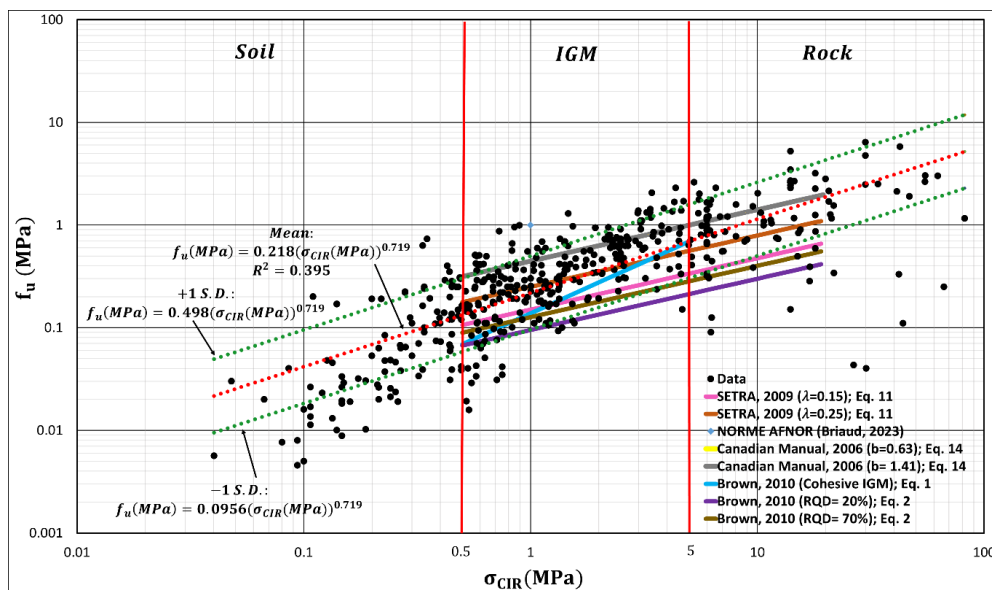


Figure 9. Evaluation of some existing guidelines to predict the ultimate side shear stress of drilled shafts.

For clays, the bearing capacity factor N_c is used to calculate the ultimate bearing pressure under the drilled shaft as $p_u = N_c (\sigma_{CIR}/2) + \gamma d$, where γ is the total unit weight of the soil and d is the embedded length of the pile; for pile depth to diameter ratio larger than 4, the N_c value is typically 9. As can be seen in Figure 10, N_c decreases with an increase in IGM strength.

Other guidelines outlined in the existing knowledge section, and using the pressuremeter limit pressure and the unconfined compression strength of the IGM, are evaluated by showing the guidelines prediction curves superimposed on the load test data in Figures 11, 12, and 13. Figure 11 compares the datapoints and prediction lines with the available design guidelines for p_u vs. σ_{CIR} . For IGM, the design guidelines align reasonably well with the data and tend to be conservative except for SETRA (2009) with RQD <10%, which is very conservative because it refers to a very weak material. Figure 12 compares datapoints and prediction lines with the available design guidelines for f_u vs. p_L ; the guidelines are reasonably conservative but are limited to p_L values less than 7 MPa. A comparison of datapoints and the Norme AFNOR design guideline for p_u vs. p_L is shown in Figure 13. The slope of the recommended line is steeper than the regression line. It could be that the p_u values were underrepresented in the database. In several load tests, the point load–settlement curves approached an asymptotic response but did not reach a clearly defined plunging failure. In such cases, p_u was estimated by extrapolating the point load–settlement curve to its asymptotic ultimate value. The extrapolation was performed only when the curve exhibited clear nonlinear softening and an identifiable trend toward limiting resistance. In this case, only the extrapolated values were used for establishing statistical correlations; this was done consistently across the database. Also, the p_u points in Figure 13 with an upward arrow indicate that the measured value was the maximum pressure applied as stated in the publication but not necessarily the ultimate value. These data were not incorporated in calculating the regression line since they had not plunged or reached the minimum 25 mm displacement.

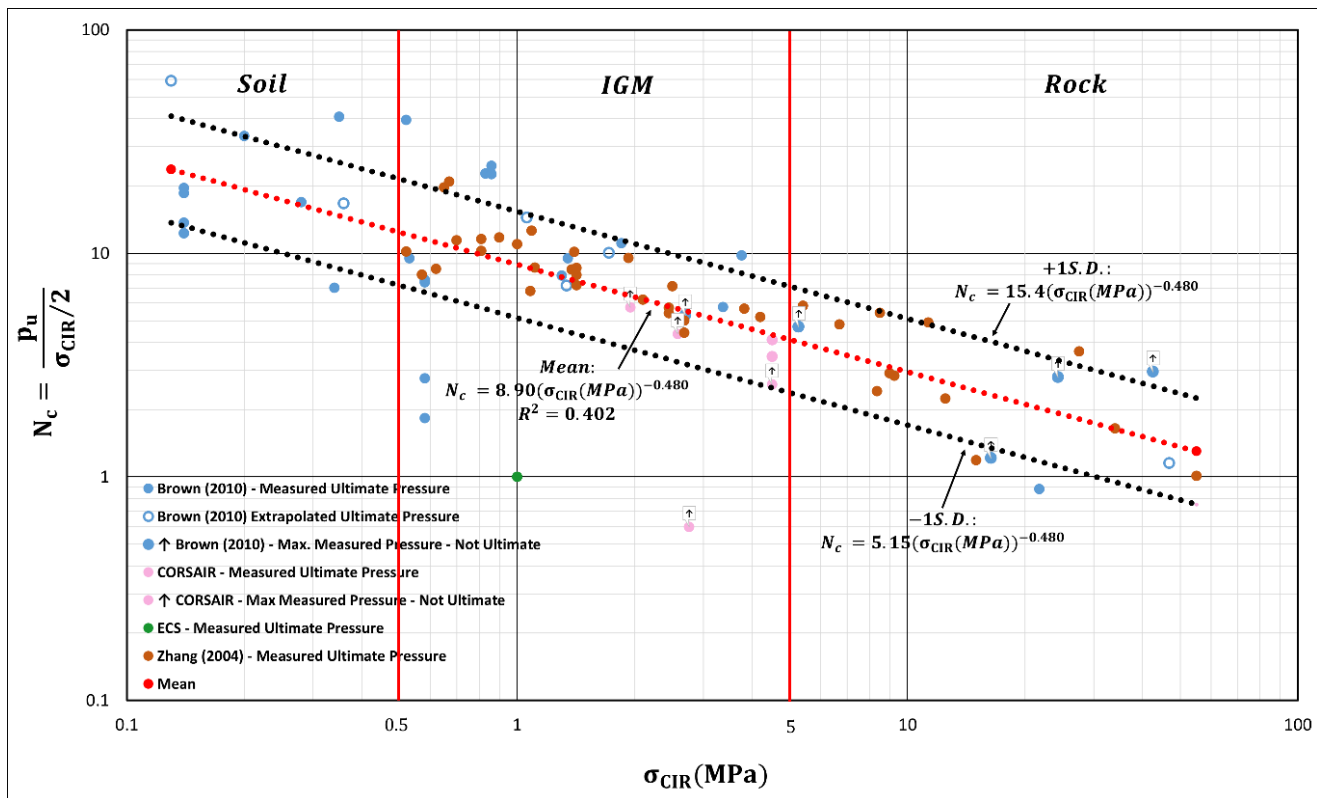


Figure 10. The N_c factor versus the unconfined compression strength for drilled shafts in IGM.

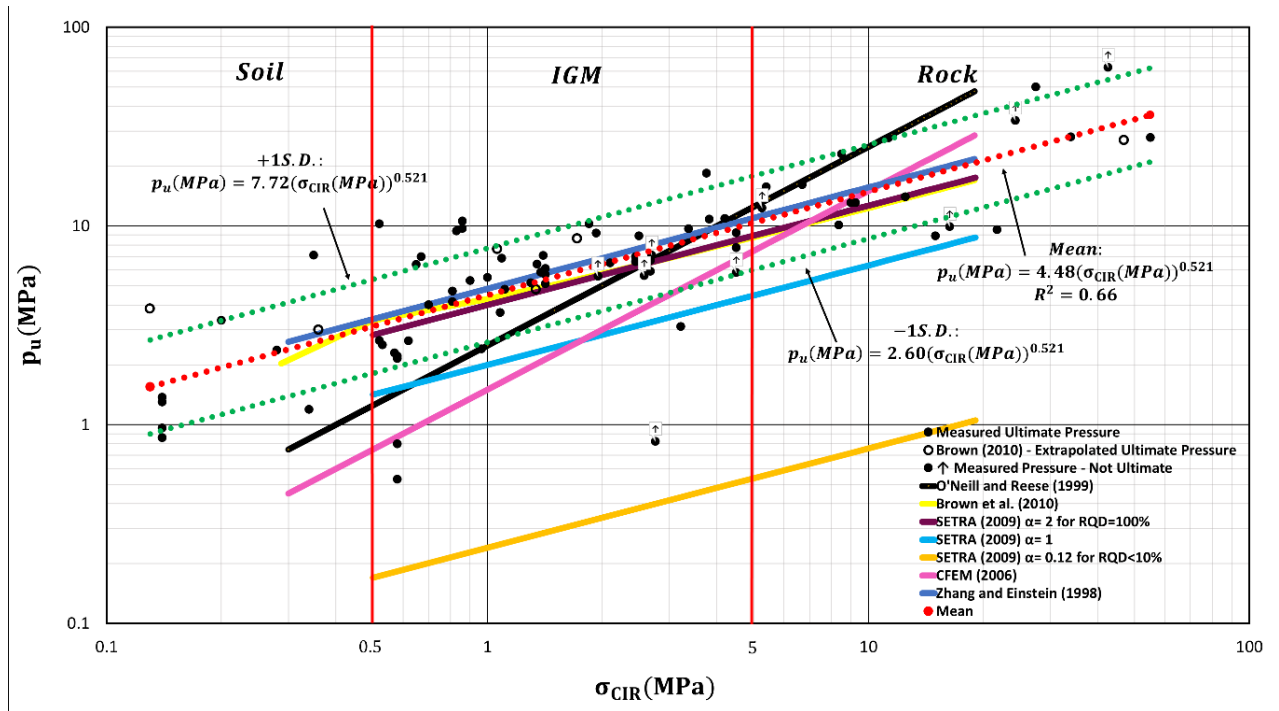


Figure 11. Evaluation of some existing guidelines to predict the ultimate point pressure of drilled shafts based on the unconfined compression strength σ_{CIR} .

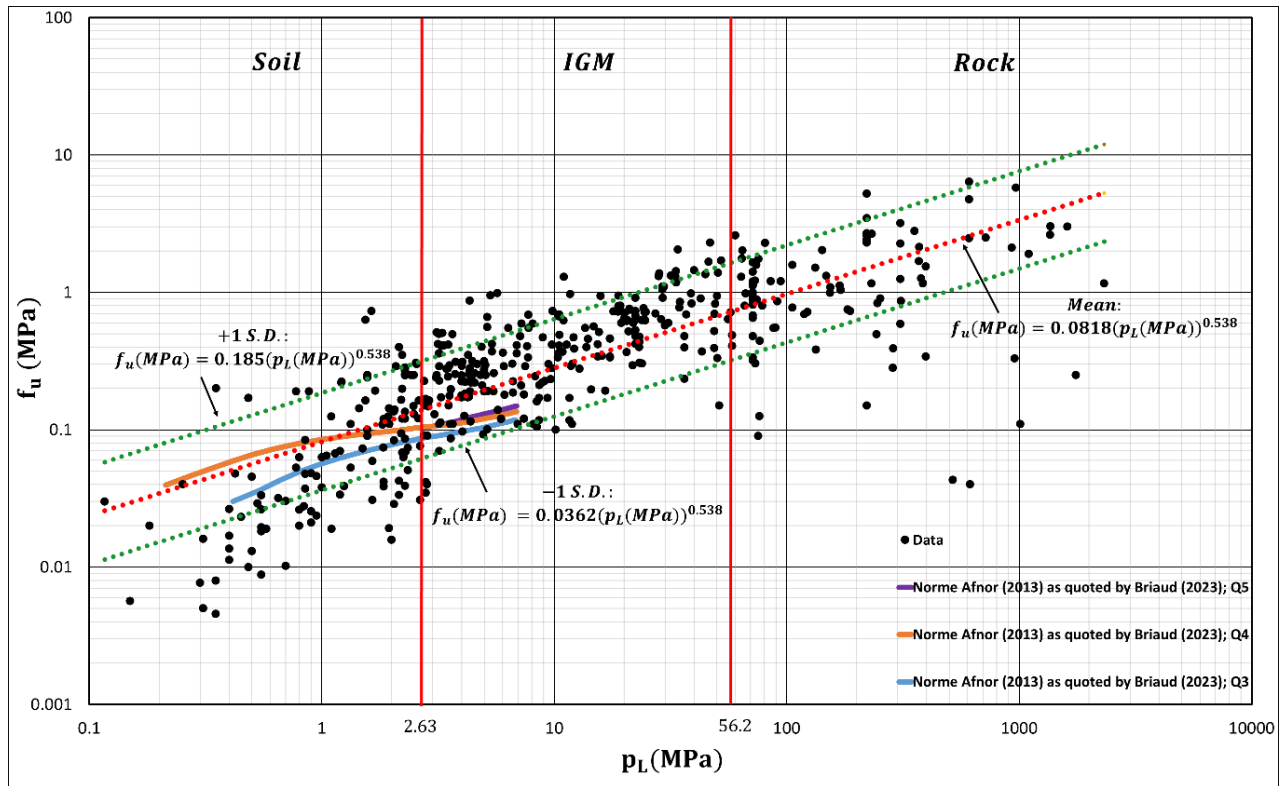


Figure 12. Evaluation of some existing guidelines to predict the ultimate side shear stress on drilled shafts based on the PMT limit pressure.

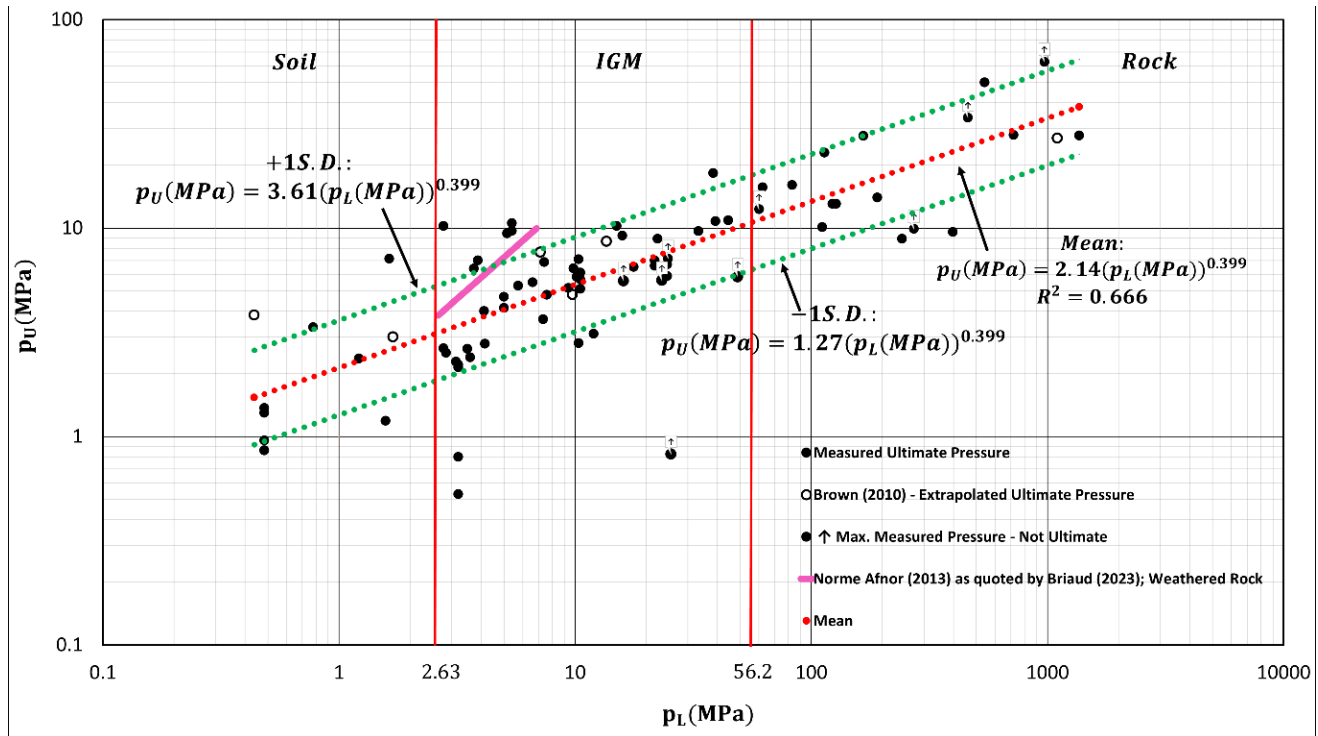


Figure 13. Evaluation of some existing guidelines to predict the ultimate point pressure of drilled shafts based on the PMT limit pressure.

CAPACITY OF DRIVEN PILES IN IGM

A database of driven pile load tests in IGM was assembled from several sources. The load tests were collected from publicly available documents (Islam et al., 2022; Ng et al., 2023, as quoted by Masud et al., 2024; Adhikari et al., 2022; Kalauni et al., 2021). The requirements were that the load tests should be on instrumented piles where the side friction and the point resistance were measured separately, that the IGM would be described including strength measurements, and that the top movement of the pile would move downward approximately one tenth of the pile diameter. A total of 49 such load tests were collected and organized; they led to 42 values of the ultimate side shear stress f_u and to 32 values of the ultimate point pressure p_u . The strength of the IGM was typically given by the unconfined compression strength of the intact IGM, σ_{CIR} . The average RQD value for each point is shown next to the data point in each plot, if available.

The ultimate side shear stress f_u was then plotted against the strength parameter of the IGM (σ_{CIR} and N). These plots are shown in Figures 14 and 15. When comparing Figures 14 and 15 to Figures 1 and 2, it is clear that the number of driven pile load tests in the database is not as large as for the drilled shaft database; this is because driven piles are not as common in IGM compared to drilled shafts. The mean regression lines were identified and gave the following expressions.

$$f_u(MPa) = 0.112(\sigma_{CIR}(MPa))^{0.186} \quad (35)$$

$$f_u(MPa) = 0.0243(N(bpf))^{0.339} \quad (36)$$

Upper and lower bounds with associated equations are shown on Figures 14 and 15 corresponding to plus and minus one standard deviation of the data. Note that the data for soils and the data for rocks is included in the figure, along with the IGM data, to emphasize the continuity of the relationship between all three main categories of earth materials.

The ultimate point pressure, p_u , was then plotted against the strength parameter of the IGM (σ_{CIR}) (Figure 16). The regression equation is shown below. No SPT blow count was available at the pile point in the IGM driven pile load test database.

$$p_u(MPa) = 7.93(\sigma_{CIR}(MPa))^{0.199} \quad (37)$$

The authors are of the opinion that the pressuremeter (PMT) is one of the best tools to obtain useful parameters for the design of deep foundations in IGM. For that reason, an effort was made to generate plots of f_u vs p_L and p_u vs p_L where p_L is the PMT limit pressure. Because no PMT data was associated with any of the load tests collected, estimates of the limit pressure were obtained from the values of σ_{CIR} using the correlation developed by Briaud (1992) (Equation 32). Then the plots of f_u vs p_L and p_u vs p_L could be generated as shown in Figures 17 and 18. The mean regression equations are:

$$f_u(MPa) = 0.086(p_L(MPa))^{0.140} \quad (38)$$

$$p_u(MPa) = 5.98(p_L(MPa))^{0.150} \quad (39)$$

A separate database was developed with CAPWAP data in IGM but is not included in this article.

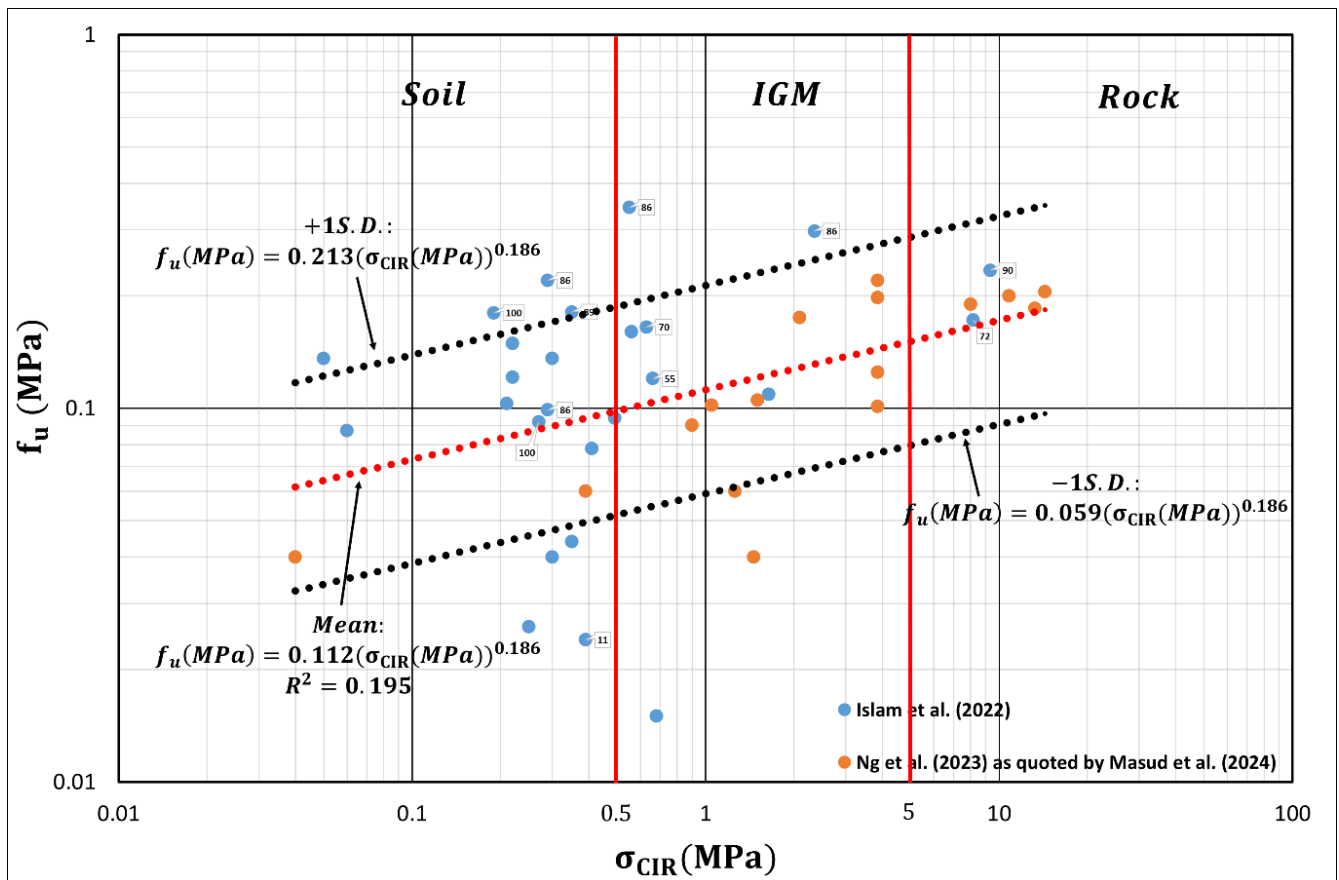


Figure 14. Ultimate side shear stress f_u versus unconfined compression strength σ_{CIR} for driven piles in IGM.

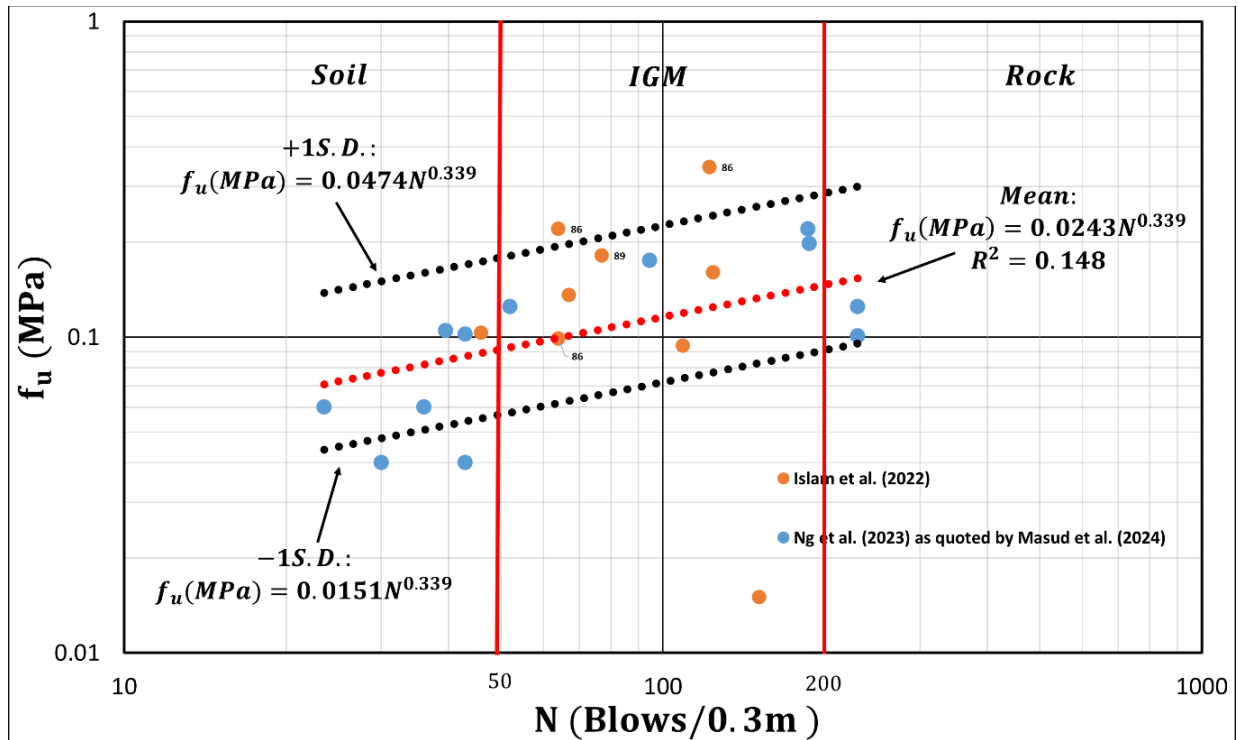


Figure 15. Ultimate side shear stress f_u versus SPT blow count N for driven piles in IGM.

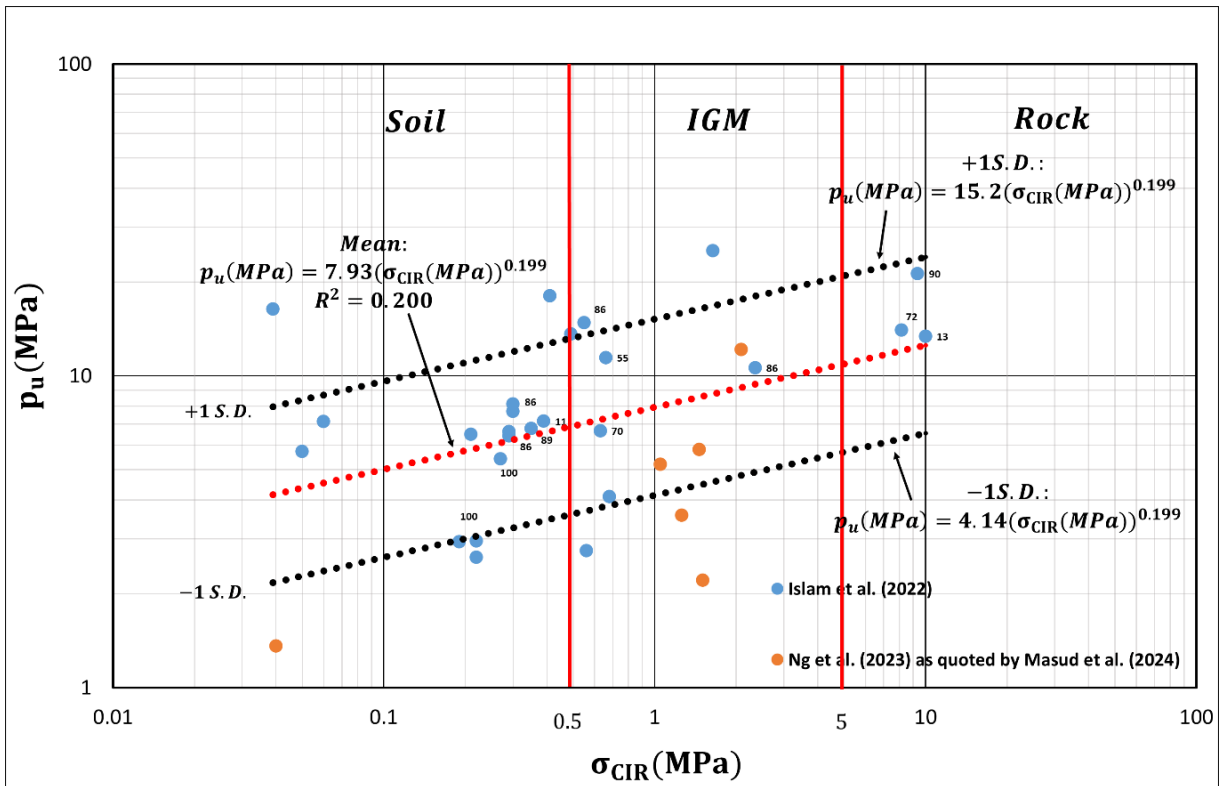


Figure 16. Ultimate point pressure p_u versus unconfined compression strength σ_{CIR} for driven piles in IGM.

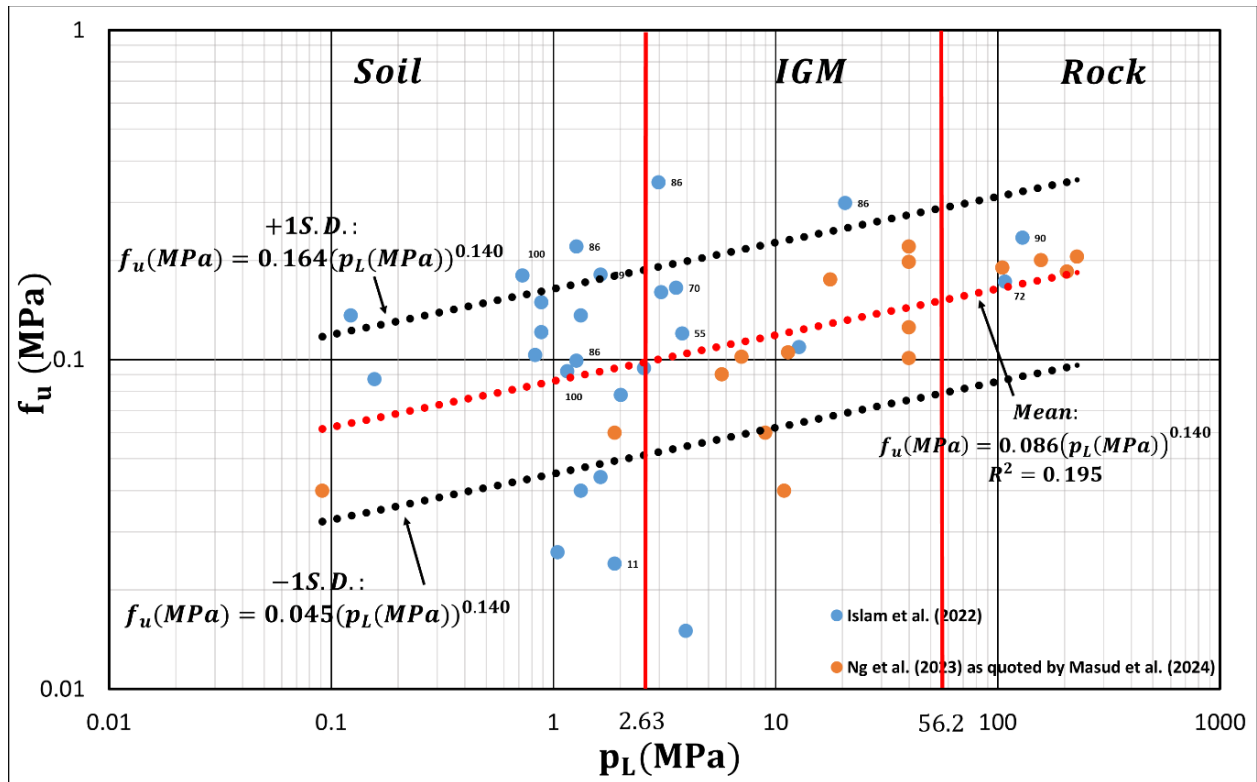


Figure 17. Ultimate side shear stress f_u versus pressuremeter limit pressure p_L for driven piles in IGM.

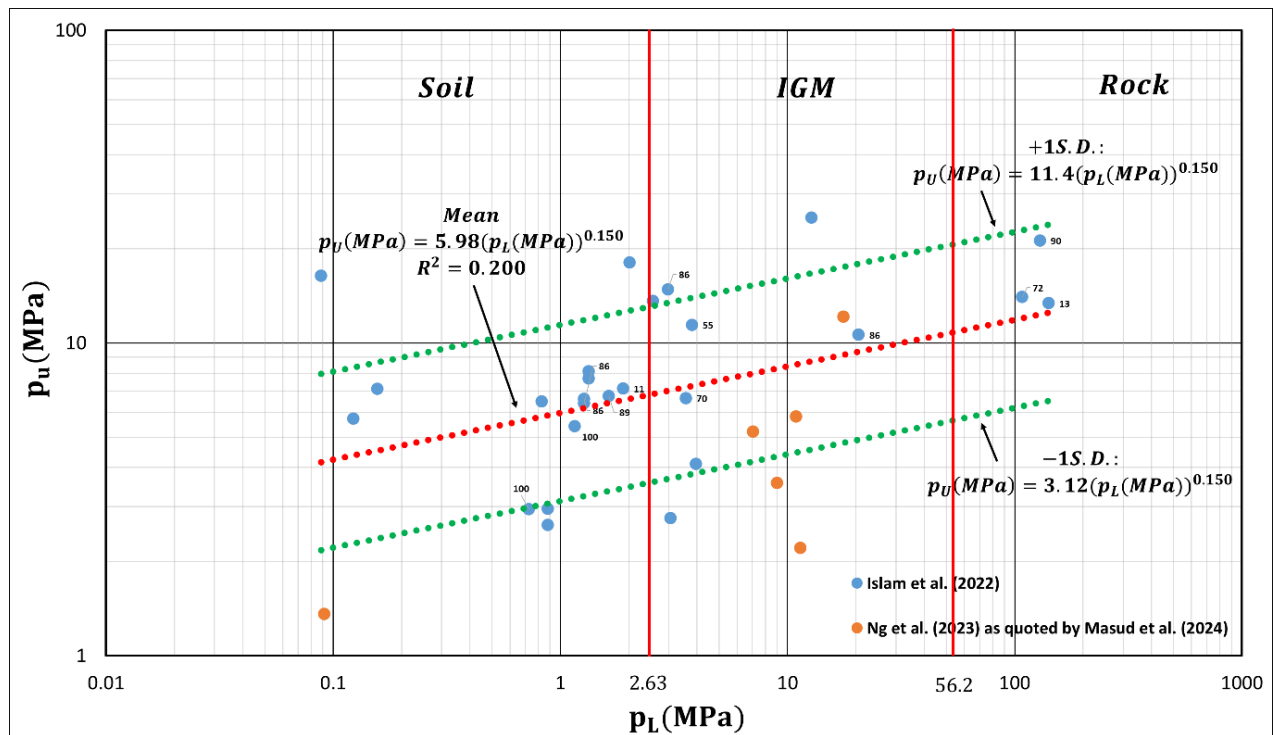


Figure 18. Ultimate point pressure p_u versus pressuremeter limit pressure p_L for driven piles in IGM.

EVALUATION OF EXISTING GUIDELINES FOR DRIVEN PILES

To evaluate some of the guidelines to estimate the ultimate side shear stress f_u and the ultimate point pressure p_u for driven piles in IGM, the recommendations outlined in the existing knowledge section are superimposed on the load tests data. Figures 19 to 21 show the results for f_u , and Figures 22 to 24 show the results for p_u . Most of the guidelines for f_u seem reasonable or conservative. However, the Meyerhoff (1976), Brown (2001), and Masoud et al. (2024) relationships in Figure 23 overpredict the measured values of p_u . This is surprising, as the relationship by Meyerhoff in particular has been well accepted in practice; this overprediction may point to a bias in the database toward lower values of p_u associated with the SPT blow count N values.

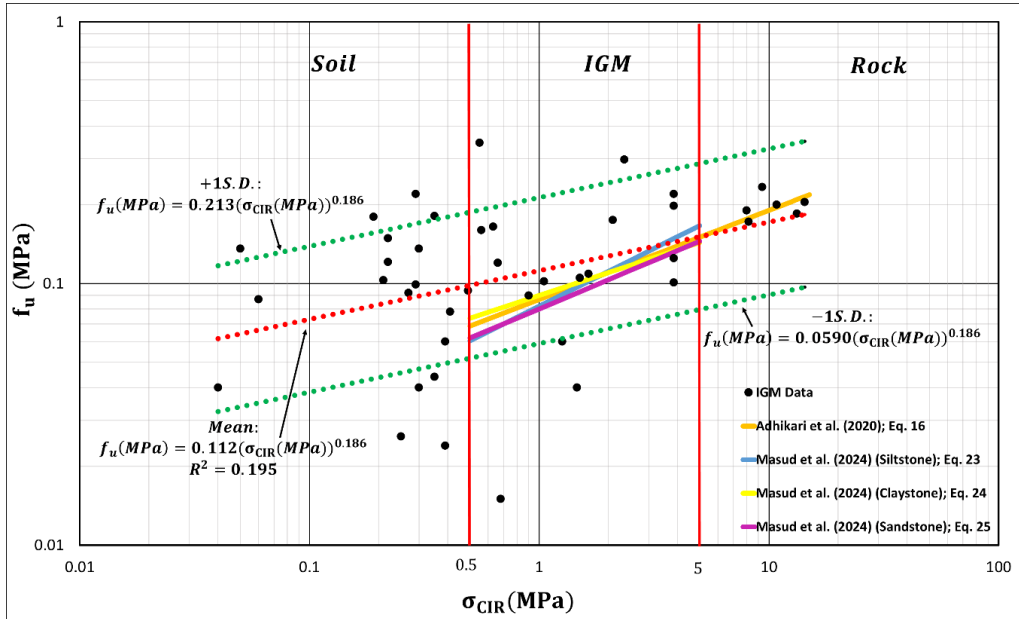


Figure 19. Evaluation of some guidelines for the ultimate side shear stress f_u versus unconfined compression strength σ_{cIR} for driven piles in IGM.

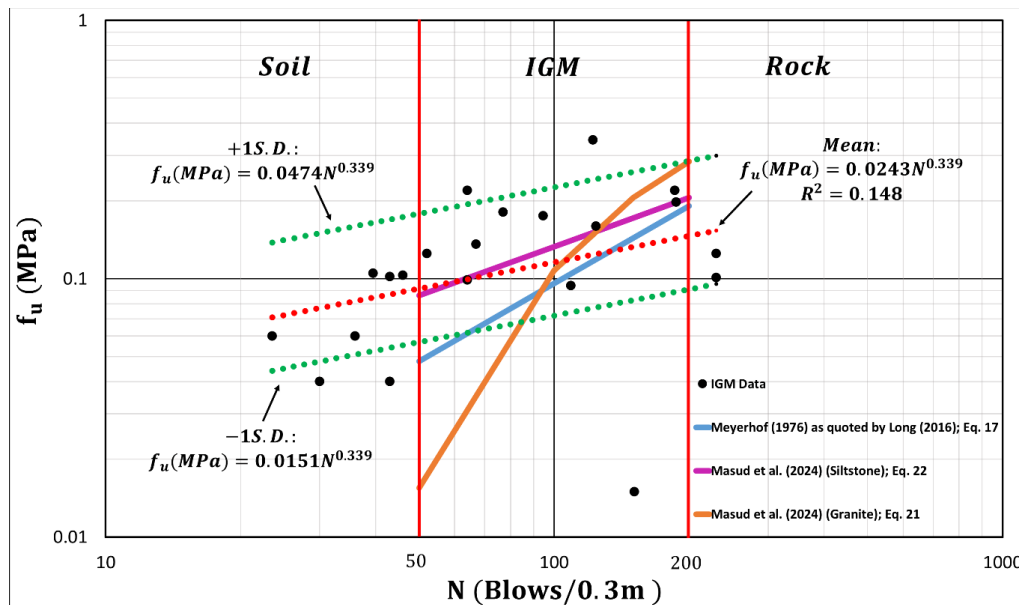


Figure 20. Evaluation of some guidelines for the ultimate side shear stress f_u versus SPT blow count N for driven piles in IGM.

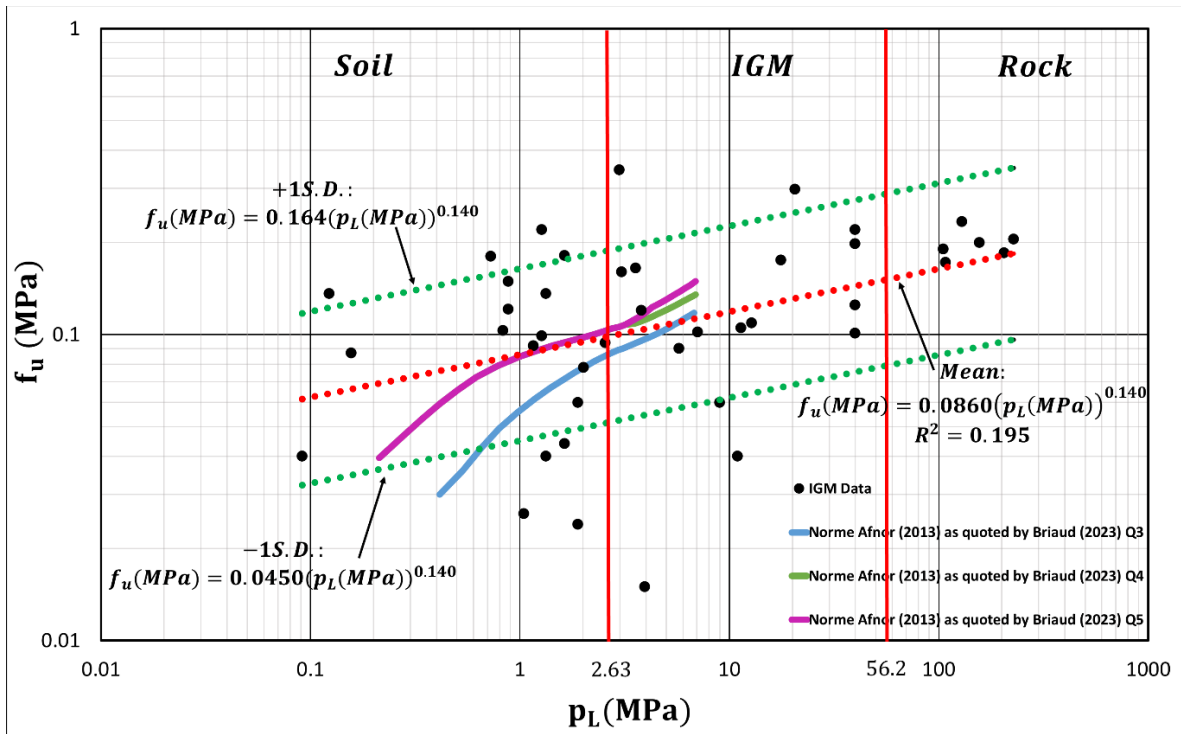


Figure 21. Evaluation of some guidelines for the ultimate side shear stress f_u versus pressuremeter limit pressure p_L for driven piles in IGM.

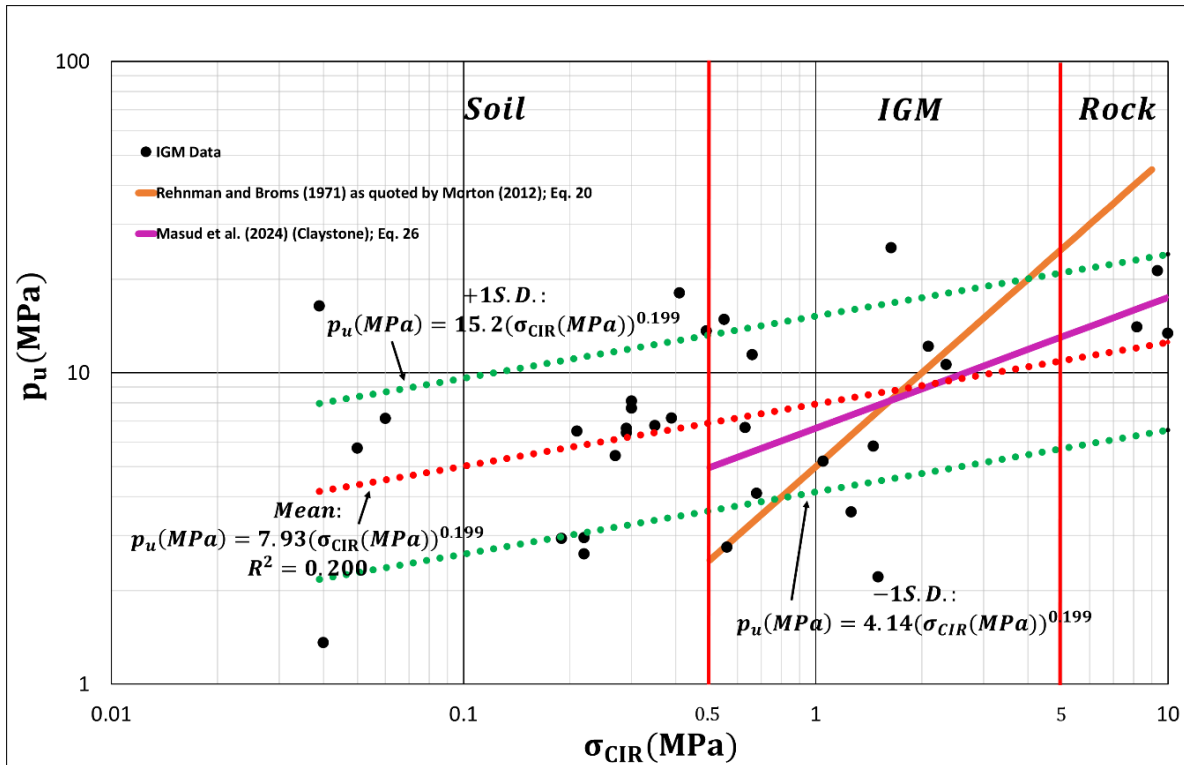


Figure 22. Evaluation of some guidelines for the ultimate point pressure p_u versus unconfined compression strength σ_{CIR} for driven piles in IGM.

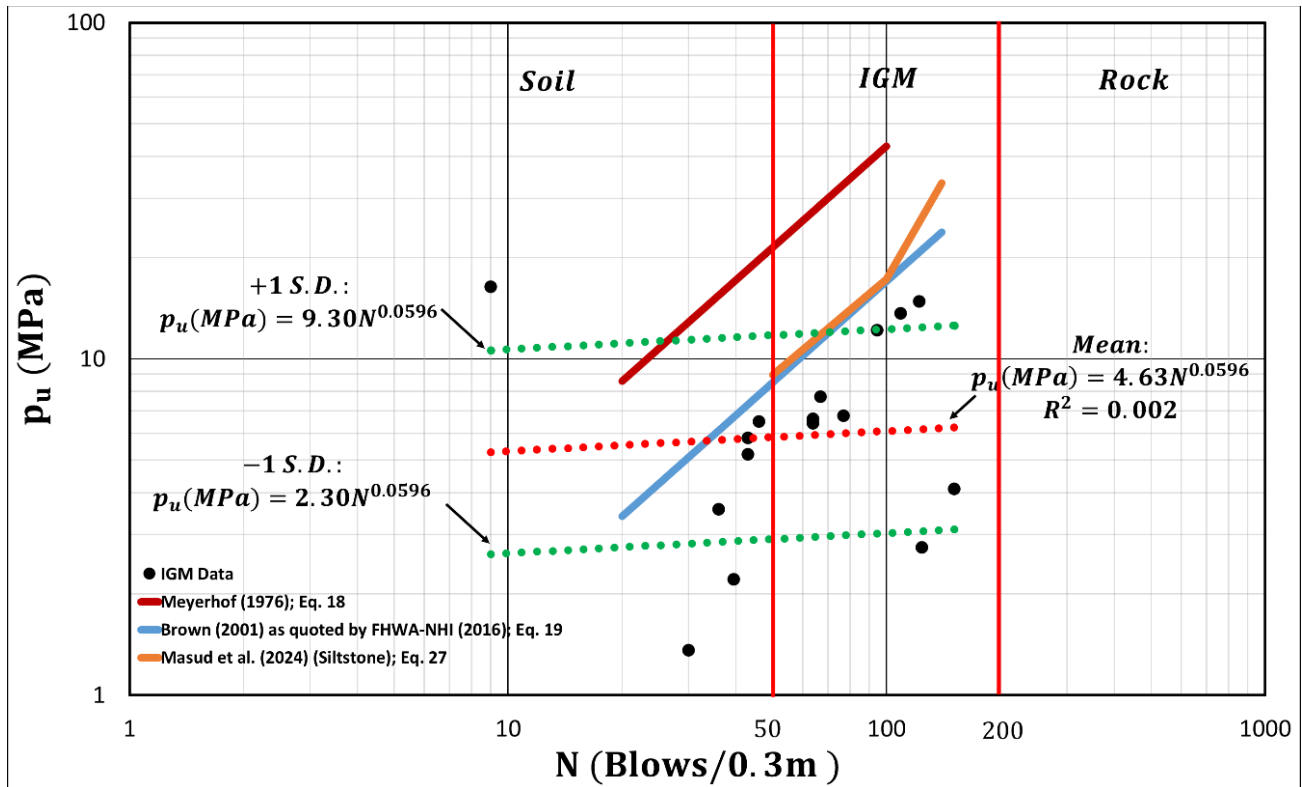


Figure 23. Evaluation of some guidelines for the ultimate point pressure p_u versus SPT blow count N for driven piles in IGM.

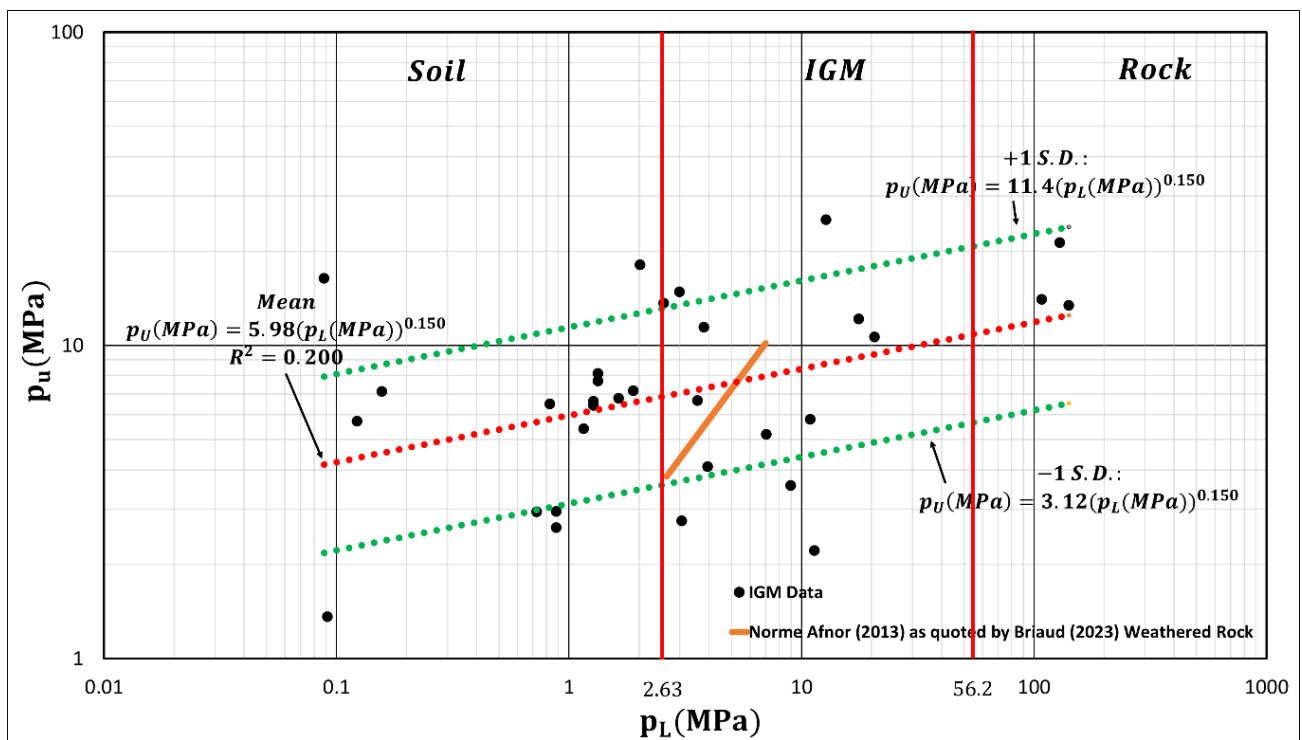


Figure 24. Evaluation of some guidelines for the ultimate point pressure p_u versus pressuremeter limit pressure p_L for driven piles in IGM.

SUMMARY AND CONCLUSIONS

The following conclusions are drawn:

1. IGM are Intermediate Geo-Materials between strong soils and soft rocks. Their properties lie somewhat outside the typical soil properties or rock properties. The unconfined compression strength of the intact material σ_{CIR} , the SPT blow count N , and the pressuremeter limit pressure p_L are selected to quantify the IGM strength.
2. A database of 318 drilled shaft instrumented load tests mostly in IGM was collected and organized. That led to 483 values of the ultimate side shear stress f_u and 84 values of the ultimate point pressure p_u .
3. A database of 49 driven pile instrumented load tests mostly in IGM was collected and organized. That led to 42 values of the ultimate side shear stress f_u and 32 values of the ultimate point pressure p_u .
4. Charts giving the ultimate side shear stress f_u and the ultimate point pressure p_u as a function of σ_{CIR} , N , and p_L are presented for IGM, along with best fit regressions. These regressions include the mean values as well as the values for plus and minus one standard deviation. These best fit regressions help the engineer select reasonable values of f_u and p_u for IGM. Unfortunately, the RQD, or other rock index of the IGM, was not sufficiently available in the publications for the RQD to help reduce the scatter in the data.
5. The charts include results for soils and for rocks and show the continuity between soils, IGMs, and rocks, of the relationships between f_u and p_u on one hand, and σ_{CIR} , N , and p_L on the other.
6. A number of IGM axial pile capacity prediction equations are evaluated by comparing them to the accumulated data. The comparisons show that:
 - a. The α value for the ultimate side shear stress f_u , which is typically between 0.5 and 1 for piles in fine grained soils, decreases as the strength of the IGM increases, and can be as low as 0.1 or less for high-strength IGM as shown in Figure 8.
 - b. The N_c bearing capacity factor in the undrained shear strength Skempton equation for the ultimate point pressure is typically taken as 9 in fine grained soils. The data in Figure 10 show that N_c decreases as the IGM strength increases, and can reach values of 2 for high-strength IGM.
 - c. Many other design recommendations, including the Canadian foundation manual, the AASHTO bridge specifications, and the French guidelines, are evaluated. They indicate which are conservative and which are optimistic. If any trend can be identified, it is that the guidelines are generally reasonable for the ultimate friction but somewhat optimistic for the ultimate point pressure.

ACKNOWLEDGEMENTS

This project was sponsored by CERGEP, the Consortium for Education and Research in Geo-Engineering Practice at Texas A&M University. The members are A.H. Beck, Corsair, ECS, Fugro, Geosyntec, Intertek-PSI, Kiewit, Menard, Odin, Paradigm, Raba Kistner, and Terracon. We wish to thank, in particular, Clint Harris at CORSAIR and Karl Higgins formerly with ECS for providing valuable load test data.

REFERENCES

- ASHTO. (1998). *LRFD bridge design specifications* (2nd ed.). American Association of Highway and Transportation Officials.
- Abu-Hejleh, N., O'Neill, M. W., Hanneman, D., & Atwooll, W. J. (2003). Improvement of the geotechnical axial design methodology for Colorado's drilled shafts socketed in weak rocks (CDOT-DTD-R-2003-6). Colorado Department of Transportation. <https://doi.org/10.1177/0361198105193600112>
- Adhikari, P., Ng, K. W., Gebreslasie, Y. Z., & Wulff, S. S. (2020). Improved α - and β -methods for the estimation of shaft resistance of steel H-piles driven into intermediate geomaterials. In *Proceedings of the Geo-Congress 2020* (pp. 114–123). American Society of Civil Engineers. <https://doi.org/10.1061/9780784482780.012>
- Adhikari, P., Ng, K. W., Gebreslasie, Y. Z., & Wulff, S. S. (2022). New static analysis methods and LRFD recommendations for steel H-piles in rock-based intermediate geomaterials. *Geotechnical and Geological Engineering*, 40(5), 2553–2567. <https://doi.org/10.1007/s10706-021-02045-x>
- Barton, N., Lien, R., & Lunde, J. (1974). Engineering classification of rock masses for the design of tunnel support. *Rock Mechanics*, 6(4), 189–236. <https://doi.org/10.1007/BF01239496>
- Bieniawski, Z. T. (1981). Experience in in situ measurements of rock deformability. *Geophysical Research Letters*, 8(7), 675–677. <https://doi.org/10.1029/GL008i007p00675>
- Bieniawski, Z. T. (1989). *Engineering rock mass classifications: A complete manual for engineers and geologists in mining, civil, and petroleum engineering*. Wiley.
- Briaud, J.-L. (1992). *The pressuremeter*. Taylor & Francis. <https://doi.org/10.1201/9780203736173>
- Briaud, J.-L. (2023). *Geotechnical engineering: Unsaturated and saturated soils* (2nd ed.). John Wiley & Sons.
- Brown, D. A., Turner, J. P., Castelli, R. J., & Americas, P. B. (2010). *Drilled shafts: Construction procedures and LRFD design methods* (FHWA-NHI-10-016). Federal Highway Administration.
- Brown, R. P. (2001). *Predicting the ultimate axial resistance of single driven piles* (Doctoral dissertation). University of Texas at Austin.
- Canadian Geotechnical Society. (2006). *Canadian foundation engineering manual* (4th ed.). BiTech Publishers.
- Deere, D. U. (1964). Technical description of rock cores for engineering purposes. *Rock Mechanics Engineering Geology*, 1, 16–22.
- Deklotz, E. J., & Boisen, B. P. (1970). Development of equipment for determining deformation modulus and in situ stresses by means of large flatjacks. In *Determination of the in situ modulus of deformation of rock masses* (ASTM STP 477, pp. 174–196). ASTM.
- Goodman, R. E., Van, T. K., & Heuze, F. E. (1968). The measurement of rock deformability in bore holes. In *Proceedings of the 10th U.S. Symposium on Rock Mech.* University of Texas.
- Hannigan, P. J., Rausche, F., Likins, G. E., Robinson, B., Becker, M., & Berg, R. R. (2016). *Design and construction of driven pile foundations—Volume I* (FHWA-NHI-16-009). National Highway Institute.
- Hoek, E. (1994). Strengths of rock and rock masses. *ISRM News J.*, 2(2), 4–16.
- Islam, M. S., Ng, K. W., & Wulff, S. S. (2022). Improved wave equation analysis of steel H-piles in shales considering LRFD and economic impact studies. *Journal of Bridge Engineering*, 27(6), 04022039. [https://doi.org/10.1061/\(ASCE\)BE.1943-5592.0001879](https://doi.org/10.1061/(ASCE)BE.1943-5592.0001879)

- Kalauni, H. K. (2021). *New static analysis methods and improved wave equation analysis program for driven piles in intermediate geomaterials with load and resistance factor design recommendations*. University of Wyoming.
- Long, J. H. (2016). *Static pile load tests on driven piles into intermediate geomaterials* (WHRP 0092-12-08). University of Illinois at Urbana-Champaign.
- Masud, N. B., Ng, K. W., Kalauni, H. K., & Wulff, S. S. (2024). Reliability-based design improvement and prediction of steel driven pile resistances in rock-based intermediate geomaterials. *Acta Geotechnica*, 19(2), 1083–1105. <https://doi.org/10.1007/s11440-023-01909-1>
- Meyerhof, G. G. (1976). Bearing capacity and settlement of pile foundations. *Journal of the Geotechnical Engineering Division*, 102(3), 197–228. <https://doi.org/10.1061/AJGEB6.0000243>
- Morton, T. S. (2012). *Assessing driven steel pile capacity on rock using empirical approaches*. Dalhousie University.
- Ng, K. W., Masud, N. B., Oluwatuyi, O. E., & Wulff, S. S. (2023). *Comprehensive field test and geotechnical investigation program for development of LRFD recommendations of driven piles on intermediate geomaterials*. Wyoming Department of Transportation.
- Association Française de Normalisation (AFNOR). (2013). *Justification des ouvrages géotechniques* (NF P 94-261; NF P 94-262). AFNOR.
- O'Neill, M. W., & Reese, L. C. (1999). *Drilled shafts: Construction procedures and design methods* (FHWA-IF-99-025). Federal Highway Administration.
- O'Neill, M. W., Townsend, F. C., Hassan, K. M., Buller, A., & Chan, P. S. (1996). *Load transfer for drilled shafts in intermediate geomaterials* (FHWA-RD-95-172). Federal Highway Administration.
- Rehman, S. E., & Broms, B. B. (1971). Bearing capacity of piles driven into rock. *Canadian Geotechnical Journal*, 8(2), 151–162. <https://doi.org/10.1139/t71-016>
- SETRA. (2009). *Fondations au rocher: Reconnaissance des massifs rocheux, conception et dimensionnement des fondations*. Cerema.
- Stark, T. D., Long, J. H., Osouli, A., & Baghdady, A. K. (2017). *Modified standard penetration test-based drilled shaft design method for weak rocks* (FHWA-ICT-17-018).
- Williams, A., & Pells, P. J. N. (1981). Side resistance rock sockets in sandstone, mudstone, and shale. *Canadian Geotechnical Journal*, 18(4), 502–513. <https://doi.org/10.1139/t81-061>
- Zhang, L. (2004). *Drilled shafts in rock: Analysis and design*. CRC Press. <https://doi.org/10.1201/9780203024423>
- Zhang, L., & Einstein, H. H. (1998). End bearing capacity of drilled shafts in rock. *Journal of Geotechnical and Environmental Engineering*, 124(7), 574–584. [https://doi.org/10.1061/\(ASCE\)1090-0241\(1998\)124:7\(574\)](https://doi.org/10.1061/(ASCE)1090-0241(1998)124:7(574)).



INTERNATIONAL JOURNAL OF GEOENGINEERING CASE HISTORIES

*The Journal's Open Access Mission is
generously supported by the following Organizations:*



Access the content of the *ISSMGE International Journal of Geoengineering Case Histories* at:
www.geocasehistoriesjournal.org